Lateral undulation of snake robots: A simplified model and fundamental properties

Pål Liljebäck, Kristin Y. Pettersen, Øyvind Stavdahl, and Jan Tommy Gravdahl

Abstract

This paper considers lateral undulation motion of snake robots. The first contribution of the paper is a model of lateral undulation dynamics developed for control design and stability analysis purposes. The second contribution is an analysis of the simplified model that shows that any asymptotically stabilizing control law for the snake robot to an equilibrium point must be time-varying. Furthermore, the analysis shows that a snake robot (with four links) is strongly accessible from almost any equilibrium point, except for certain singular configurations, and that the robot does not satisfy sufficient conditions for small-time local controllability (STLC). The third contribution is based on using averaging theory to prove that the average velocity of the robot during lateral undulation will converge exponentially fast to a steady state velocity which is given analytically as a function of the gait pattern parameters. From the averaging analysis, we also derive a set of fundamental relationships between the gait parameters of lateral undulation and the resulting forward velocity of the snake robot. The paper presents simulation results and results from experiments with a physical snake robot that support the theoretical findings.

I. INTRODUCTION

Inspired by biological snake locomotion, snake robots carry the potential of meeting the growing need for robotic mobility in unknown and challenging environments. These mechanisms typically consist of serially connected joint modules capable of bending in one or more planes. The many degrees of freedom

Affiliation of Pål Liljebäck is shared between the Dept. of Engineering Cybernetics at the Norwegian University of Science and Technology (NTNU), NO-7491 Trondheim, Norway, and SINTEF ICT, Dept. of Applied Cybernetics, N-7465 Trondheim, Norway. E-mail: Pal.Liljeback@sintef.no.

Kristin Y. Pettersen, Øyvind Stavdahl, and Jan Tommy Gravdahl are with the Dept. of Engineering Cybernetics at the Norwegian University of Science and Technology (NTNU), NO-7491 Trondheim, Norway. E-mail: {Kristin.Y.Pettersen, Oyvind.Stavdahl, Tommy.Gravdahl}@itk.ntnu.no.

of snake robots make them difficult to control, but provide traversability in irregular environments that surpasses the mobility of the more conventional wheeled, tracked and legged forms of robotic mobility.

There are several reported works aimed at analysing and understanding snake locomotion. Gray[1] conducted empirical and analytical studies of snake locomotion already in the 1940s. Hirose[2] studied biological snakes and developed mathematical relationships characterizing their motion, such as the *serpenoid curve*. Chirikjian[3;4] modelled the kinematics of snake robots in terms of continuous backbone curves that capture the macroscopic geometry of the robot. Gaits for the backbone curve were specified with respect to environment constraints and the desired locomotion trajectory of the robot. Ostrowski[5] studied the controllability properties of a wheeled snake robot on a kinematic level. Prautsch *et al.*[6] modelled the dynamics of a wheeled snake robot and proposed an asymptotically stable controller for the position of the robot. Ma[7] modelled a planar snake robot without wheels and optimized the motion of the robot based on computer simulations. Date *et al.*[8] developed controllers for wheeled snake robots aimed at minimizing the lateral constraint forces on the wheels of the robot during locomotion. Saito *et al.*[9] modelled a planar snake robot and optimized the parameters of Hirose's serpenoid curve based on simulations. Hicks[10] investigated general requirements for the propulsion of a three-linked snake robot. Nilsson[11] employed energy arguments to analyse planar snake locomotion under isotropic friction conditions. Matsuno and Sato[12] considered trajectory tracking of snake robots where some, but not all, of the links were assumed to be wheeled. Transeth *et al.*[13] proved that the translational and rotational velocity of a planar snake robot is bounded. Li *et al.*[14] studied the controllability of the joint motion of a snake robot, but did not consider the position and orientation of the robot. Hu *et al.*[15] investigated the frictional properties of snake skin both mathematically and experimentally, and showed that the friction coefficients of a snake in the transversal and tangential direction of the body, respectively, are different. The study also showed that the weight distribution of a snake during lateral undulation is not uniform, but rather distributed so that the peaks of the body wave curve are slightly lifted from the ground. Hatton[16] introduced the concept of a body velocity integral in order to easily approximate the net displacement of a snake robot during a gait. The method requires that the system coordinates are properly chosen. The authors have previously studied the stability properties of snake locomotion based on *Poincaré maps* and investigated the controllability properties of a planar snake robot influenced by anisotropic friction[17].

Research on control of robotic fish and eel-like mechanisms is relevant to research on snake robots since these mechanisms are very similar. Vela *et al.*[18], McIsaac and Ostrowski[19], and Morgansen *et al.*[20] investigate the controllability of various fish-like mechanisms, synthesize gaits for translational and rotational motion based on Lie bracket calculations, and propose controllers for tracking straight and

curved trajectories.

The understanding of snake locomotion so far is for the most part based on empirical studies of biological snakes and simulation-based synthesis of relationships between parameters of the snake. This is due to the complexity of existing models of snake locomotion. This paper is an attempt to contribute to the understanding of snake robot locomotion through systematic analytical investigations of the equations of motion of such mechanisms. In particular, this paper considers the dynamics of snake robots moving according to the gait pattern *lateral undulation*, which is the most common form of snake locomotion.

The paper has three distinct contributions. The first contribution is a *simplified model* of lateral undulation dynamics developed to facilitate synthesis of new control strategies for snake robots. The model is developed based on an analysis of an existing complex model of a snake robot that identifies a set of essential properties of lateral undulation. The basic idea behind the simplified model is to capture only these essential properties of the snake robot dynamics, i.e. the features that determine the overall behaviour of the snake. The main difference between the simplified model and previous models proposed in the snake robot literature concerns the choice of body shape coordinates. In particular, previous models describe the body shape dynamics in terms of the *rotational* motion of the links of the snake robot, which generally results in complex equations of motion which are challenging to analyse from a motion control perspective. The model proposed in this paper, on the other hand, describes the body shape dynamics in terms of the *translational* motion of the links, which significantly simplifies the equations of motion. Note that there are several limitations of this modelling approach, which are elaborated in the paper. The modelling approach is for instance limited to snake locomotion where the link angles are limited.

The second contribution is an analysis of the simplified model that shows that any asymptotically stabilizing feedback control law for the snake robot to an equilibrium point must be time-varying. Furthermore, the analysis shows that the snake robot is strongly accessible from almost any equilibrium point, except for certain singular configurations, and that the robot does not satisfy sufficient conditions for small-time local controllability (STLC). These conclusions agree with a similar analysis presented by the authors[21], which was based on a more complex model of snake locomotion.

The third contribution is based on using averaging theory to investigate the velocity dynamics of the snake robot during lateral undulation. The average velocity of the snake robot is shown to converge exponentially fast to a steady state velocity, and an analytical expression for calculating the steady state velocity is presented as a function of the various controller parameters. To the authors' best knowledge, this is the first time the steady state velocity of a wheel-less snake robot with anisotropic ground friction properties is derived analytically in terms of the gait pattern parameters. The averaging analysis also

reveals a set of fundamental relationships between the gait parameters of lateral undulation and the resulting forward velocity of the snake robot that are useful from a motion planning perspective. The derived properties state that the average forward velocity of a planar snake robot 1) is proportional to the squared amplitude of the sinusoidal motion of each joint, 2) is proportional to the angular frequency of the sinusoidal motion of each joint, 3) is proportional to a particular function of the constant phase shift between the joints, and 4) is maximized by the phase shift between the joints that also maximizes the particular phase shift function. Note that the linear relationships under item 1) and 2) have been shown in previous literature, for instance in the context of modelling and control of swimming robots[19;22;23;24].

Each of the contributions described above are accompanied by simulation results that support the theoretical findings. In addition, the derived relationships between the gait parameters of lateral undulation and the resulting forward velocity are validated through experiments with a physical snake robot.

Note that this paper is based on and extends previous preliminary work by the authors[25;26;27;28]. The extensions in this paper include an improved analytical justification of the simplified model, an improved specification of the validity of the model, improved simulation results which illustrate the limitations of the simplified modelling approach, and general improvements that provide a united presentation of the results and the relations between them.

The paper is organized as follows. Section II presents an existing complex model of a snake robot. The gait pattern lateral undulation is presented in Section III. Section IV analyses the complex model in order to identify fundamental properties of lateral undulation motion, and these properties are used in Section V to develop a simplified model of a snake robot during lateral undulation motion. Section VI investigates the stabilizability properties of a snake robot described by the simplified model, while the controllability properties are investigated in Section VII. Section VIII derives fundamental properties of the velocity dynamics of the snake robot based on averaging theory. Sections IX, X, and XI present simulation results in order to support the validity of the theoretical findings, while Section XII presents experimental results in order to investigate the validity of the derived properties of the velocity dynamics. Finally, Section XIII presents some concluding remarks.

II. A COMPLEX MODEL OF A PLANAR SNAKE ROBOT

This section summarizes an existing complex model of a planar snake robot[17]. The model will be analysed in Section IV in order to identify some essential properties of lateral undulation motion. This analysis will be used as a basis for the development of a simplified model of lateral undulation dynamics in Section V.
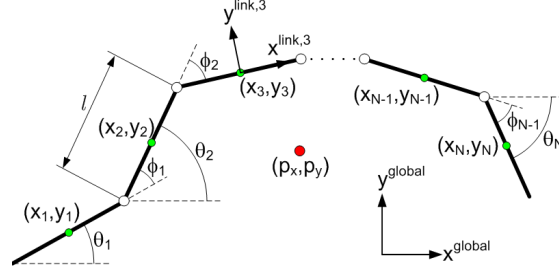
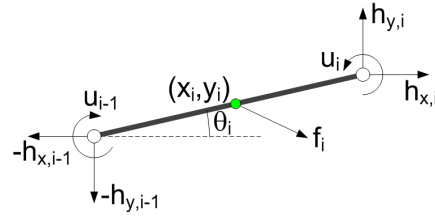Fig. 1.   Kinematic parameters of the snake robot.

Fig. 2.   Forces and torques acting on each link of the snake robot.

A. Notation and defined symbols

We consider a planar snake robot consisting of N links of length l interconnected by $N-1$ active joints. The kinematics and dynamics of the snake robot are defined in terms of the mathematical symbols described in Table I and illustrated in Fig. 1 and Fig. 2. All N links have the same mass m and moment of inertia J. The total mass of the snake robot is therefore Nm. The mass of each link is uniformly distributed so that the link CM (center of mass) is located at its center point.

The snake robot moves in the horizontal plane and has a total of $N + 2$ degrees of freedom. The position of the CM (center of mass) of the snake robot is denoted by $\boldsymbol{p} = (p_x, p_y) \in \mathbb{R}^2$. The absolute angle θ_i of link i is expressed with respect to the global x axis with counterclockwise positive direction. As seen in Fig. 1, the relative angle between link i and link $i + 1$ is given by $\phi_i = \theta_{i+1} - \theta_i$. The local coordinate system of each link is fixed in the CM of the link with x (tangential) and y (normal) axis oriented such that they are oriented in the directions of the global x and y axis, respectively, when the link angle is zero. The rotation matrix from the global frame to the frame of link i is given by

$$\boldsymbol{R}_{\text{link},i}^{\text{global}} = \begin{bmatrix} \cos\theta_i & -\sin\theta_i \\ \sin\theta_i & \cos\theta_i \end{bmatrix} \qquad (1)$$

TABLE I

PARAMETERS THAT CHARACTERIZE THE SNAKE ROBOT.

Symbol	Description
N	Number of links.
l	Length of a link.
m	Mass of each link.
J	Moment of inertia of each link.
θ_i	Angle between link i and the global x axis.
ϕ_i	Angle of joint i.
(x_i, y_i)	Global coordinates of the CM of link i.
(p_x, p_y)	Global coordinates of the CM of the robot.
u_i	Actuator torque at joint i.
$(f_{x,i}, f_{y,i})$	Ground friction force on link i in the global frame.
$(h_{x,i}, h_{y,i})$	Joint constraint force on link i from link $i+1$.
$-(h_{x,i-1}, h_{y,i-1})$	Joint constraint force on link i from link $i-1$.

The forces and torques acting on link i are visualized in Fig. 2. The ground friction force is denoted by f_i and acts on the CM of the link. The joint constraint forces from link $i+1$ and link $i-1$ are denoted by $(h_{x,i}, h_{y,i}) \in \mathbb{R}^2$ and $(-h_{x,i-1}, -h_{y,i-1}) \in \mathbb{R}^2$, respectively. The actuator torque applied at joint i is denoted by u_i.

B. Ground friction model

In this paper, we consider snake robots influenced by *viscous* ground friction forces. A *Coulomb* friction model, which assumes that the ground friction force on a link is proportional to the weight of the link, is more accurate (from a physical point of view) than a viscous friction model. However, the predominant factor which propels a planar snake robot forward during lateral undulation is the *anisotropic* ground friction property of the links[15], i.e. the property that the friction coefficients of a link in its tangential and normal direction, respectively, are different. This friction property, which is exhibited by biological snakes and also assumed in the majority of published research on snake robots, is independent of the choice of ground friction model. We therefore conjecture that the motion of a snake robot is qualitatively (although not quantitatively) similar with anisotropic viscous friction as with anisotropic Coulomb friction.

Moreover, a viscous friction model is far less complex than a Coulomb friction model, which makes the viscous model more suitable for control design and analysis purposes.

The viscous ground friction is characterized by the two friction coefficients c_t and c_n describing the friction force in the tangential (along link x axis) and normal (along link y axis) direction of a link, respectively. Using (1), the viscous friction force on link i in the global frame, denoted by $\boldsymbol{f}_i \in \mathbb{R}^2$, can be written as a function of the global link velocities, $\dot{x}_i$ and $\dot{y}_i$, as

$$
\begin{aligned}
\boldsymbol{f}_i &= \boldsymbol{R}_{\text{link},i}^{\text{global}} \boldsymbol{f}_i^{\text{link},i} = -\boldsymbol{R}_{\text{link},i}^{\text{global}} \begin{bmatrix} c_t & 0 \\ 0 & c_n \end{bmatrix} \boldsymbol{v}_i^{\text{link},i} \\
&= -\boldsymbol{R}_{\text{link},i}^{\text{global}} \begin{bmatrix} c_t & 0 \\ 0 & c_n \end{bmatrix} \left(\boldsymbol{R}_{\text{link},i}^{\text{global}} \right)^T \begin{bmatrix} \dot{x}_i \\ \dot{y}_i \end{bmatrix}
\end{aligned}
\tag{2}
$$

where $\boldsymbol{f}_i^{\text{link},i}$ and $\boldsymbol{v}_i^{\text{link},i}$ are, respectively, the friction force and the link velocity expressed in the local link frame. This gives

$$
\boldsymbol{f}_i = \begin{bmatrix} f_{x,i} \\ f_{y,i} \end{bmatrix} = - \begin{bmatrix} F_x(\theta_i) & F_{xy}(\theta_i) \\ F_{xy}(\theta_i) & F_y(\theta_i) \end{bmatrix} \begin{bmatrix} \dot{x}_i \\ \dot{y}_i \end{bmatrix}
\tag{3}
$$

where

$$
F_x(\theta_i) = c_t \cos^2 \theta_i + c_n \sin^2 \theta_i
\tag{4a}
$$

$$
F_{xy}(\theta_i) = (c_t - c_n) \sin \theta_i \cos \theta_i
\tag{4b}
$$

$$
F_y(\theta_i) = c_t \sin^2 \theta_i + c_n \cos^2 \theta_i
\tag{4c}
$$

C. Equations of motion

As shown in previous work by the authors[17], the equations of motion of the snake robot in terms of the joint angles $\boldsymbol{\phi} \in \mathbb{R}^{N-1}$, the absolute angle of the head link $\theta_N \in \mathbb{R}$, the position of the CM of the snake robot $(p_x, p_y) \in \mathbb{R}^2$, and a transformed control input $\overline{\boldsymbol{u}} \in \mathbb{R}^{N-1}$, can be written as

$$
\ddot{\boldsymbol{\phi}} = \overline{\boldsymbol{u}}
\tag{5a}
$$

$$
\ddot{\theta}_N = g(\boldsymbol{\phi}, \theta_N, \dot{\boldsymbol{\phi}}, \dot{\theta}_N, \dot{p}_x, \dot{p}_y, \overline{\boldsymbol{u}})
\tag{5b}
$$

$$
Nm\ddot{p}_x = \sum_{i=1}^{N} f_{x,i}
\tag{5c}
$$

$$
Nm\ddot{p}_y = \sum_{i=1}^{N} f_{y,i}
\tag{5d}
$$

where $g(\boldsymbol{\phi}, \theta_N, \dot{\boldsymbol{\phi}}, \dot{\theta}_N, \dot{p}_x, \dot{p}_y, \overline{\boldsymbol{u}}) \in \mathbb{R}$ is a function of the state vector and the joint torques. The ground friction force on each link, represented by $f_{x,i}$ and $f_{y,i}$, is the viscous friction force defined in (3). The model of snake locomotion given by (5) will not be detailed further here, but we note that the model is very complex from a stability analysis perspective. This complexity is the main motivation behind the simplified model developed in Section V.

III. THE GAIT PATTERN LATERAL UNDULATION

Lateral undulation, also called serpentine crawling, is the fastest and most common form of snake locomotion. During lateral undulation, continuous horizontal waves are propagated backwards along the snake body from head to tail. The body waves produce interaction forces between the snake body and irregularities in the surface that push the snake forward. As proposed by Hirose[2], lateral undulation is achieved by controlling joint $i \in \{1, \cdots, N-1\}$ of the snake robot according to the sinusoidal reference

$$\phi_{i,\mathrm{ref}} = \alpha \sin\left(\omega t + (i-1)\delta\right) + \phi_o \tag{6}$$

where α and ω are the amplitude and frequency, respectively, of the sinusoidal joint motion and δ determines the phase shift between the joints. The parameter ϕ_o is a joint offset coordinate used to control the direction of the locomotion. In this paper, we will assume that ϕ_o is a constant offset, so that

$$\dot{\phi}_{i,\mathrm{ref}} = \alpha\omega \cos\left(\omega t + (i-1)\delta\right) \tag{7}$$

$$\ddot{\phi}_{i,\mathrm{ref}} = -\alpha\omega^2 \sin\left(\omega t + (i-1)\delta\right) \tag{8}$$

To make the joints of the snake robot track the reference angles $\boldsymbol{\phi}_{\mathrm{ref}} = [\phi_{1,\mathrm{ref}}, \cdots, \phi_{N-1,\mathrm{ref}}]^T \in \mathbb{R}^{N-1}$ defined in (6), we set the control input $\overline{\boldsymbol{u}}$ according to the control law

$$\overline{\boldsymbol{u}} = \ddot{\boldsymbol{\phi}}_{\mathrm{ref}} + k_d\left(\dot{\boldsymbol{\phi}}_{\mathrm{ref}} - \dot{\boldsymbol{\phi}}\right) + k_p\left(\boldsymbol{\phi}_{\mathrm{ref}} - \boldsymbol{\phi}\right) \tag{9}$$

where $k_p > 0$ and $k_d > 0$ are scalar controller gains. By inserting (9) into (5a), the error dynamics of the joints is given by

$$\left(\ddot{\boldsymbol{\phi}}_{\mathrm{ref}} - \ddot{\boldsymbol{\phi}}\right) + k_d\left(\dot{\boldsymbol{\phi}}_{\mathrm{ref}} - \dot{\boldsymbol{\phi}}\right) + k_p\left(\boldsymbol{\phi}_{\mathrm{ref}} - \boldsymbol{\phi}\right) = \mathbf{0} \tag{10}$$

which is clearly *exponentially stable*[29].

IV. ANALYSIS OF LATERAL UNDULATION BASED ON THE COMPLEX MODEL

This section analyses the complex model given by (5) in order to identify a set of properties that characterize the motion of a planar snake robot conducting lateral undulation. These properties will be used as a basis for the development of a simplified model of lateral undulation motion in Section V.
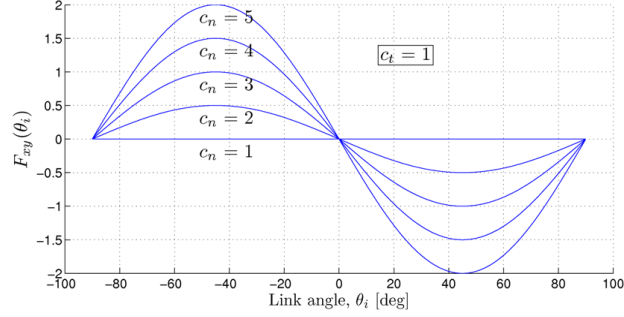
Fig. 3. The mapping from sideways link motion to forward propulsion for different viscous friction coefficients.

A. Analysis of propulsive forces during snake locomotion

We begin by investigating how a snake robot described by (5) is able to propel itself forward. We assume that the forward direction of motion is along the global positive x axis. The total force propelling the CM (center of mass) of the robot forward is therefore given from (5c) as

$$Nm\ddot{p}_x = \sum_{i=1}^{N} f_{x,i} \tag{11}$$

Wee see that the total *propulsive force* on the snake robot is simply the sum of all external forces in the global x direction. Inserting the expression for $f_{x,i}$ from (3) gives

$$Nm\ddot{p}_x = -\sum_{i=1}^{N} F_x(\theta_i)\dot{x}_i - \sum_{i=1}^{N} F_{xy}(\theta_i)\dot{y}_i \tag{12}$$

It is seen from (12) that the total propulsive force consists of two components, i.e. one involving the linear velocities of the links in the *forward* direction of motion, $F_x(\theta_i)\dot{x}_i$ (since we assume that the forward direction is along the x axis), and one involving the linear velocities *normal* to the direction of motion, $F_{xy}(\theta_i)\dot{y}_i$. $F_x(\theta_i)$ is given by (4a) and is clearly always positive. Furthermore, we assume that $\dot{x}_i > 0$ when the snake robot is moving forward ($\dot{p}_x > 0$), which is a valid assumption as long as the link angle amplitudes are limited. Due to the minus signs in (12), this means that the component $F_x(\theta_i)\dot{x}_i$ is *not* contributing to the forward propulsion of the robot, but rather opposing it. This is also expected since the snake robot must naturally be subjected to a friction force in the opposite direction of the motion.

Any propulsive force on the snake robot must therefore be produced by the *sideways* motion of the links, i.e. the product $F_{xy}(\theta_i)\dot{y}_i$. A plot of $F_{xy}(\theta_i)$ for different values of the normal friction coefficient c_n, while keeping the tangential friction coefficient c_t fixed, is shown in Fig. 3. For each plot, the angle between the link and the forward direction, θ_i, is varied from $-90°$ to $90°$. The sideways motion of the

links have no effect on the propulsive force on the snake robot when the friction coefficients are equal since this gives $F_{xy}(\theta_i) = 0$. However, when $c_n > c_t$, Fig. 3 reveals that $F_{xy}(\theta_i)$ is negative as long as θ_i is positive, and vice versa. With reference to (12), this means that the sideways motion of link i produces a positive contribution to the propulsion of the snake robot through the product $F_{xy}(\theta_i)\dot{y}_i$ as long as $\mathrm{sgn}(\theta_i) = \mathrm{sgn}(\dot{y}_i)$.

The function $F_{xy}(\theta_i)$ can be viewed as a mapping from link velocities normal to the direction of motion into force components in the direction of motion. The extrema of $F_{xy}(\theta_i)$ occur at $\theta_i = \pm 45°$. This means that, for a given $\dot{y}_i$, a link produces its highest propulsive force when it forms an angle of $\pm 45°$ with the forward direction of motion.

The above analysis is summarized by the following properties of planar snake locomotion under viscous friction conditions:

Property 1: For a snake robot described by (5) with $c_n > c_t$, forward propulsion is produced by the link velocity components that are normal to the forward direction.

Property 2: For a snake robot described by (5) with $c_n > c_t$, the propulsive force generated by the transversal motion of link i is positive as long as $\mathrm{sgn}(\theta_i) = \mathrm{sgn}(\dot{y}_i)$.

Property 3: For a snake robot described by (5) with $c_n > c_t$, the magnitude of the propulsive force produced by link i increases when $|\theta_i|$ increases as long as $|\theta_i| < 45°$.

Note that these results are general in the sense that we have not yet made any assumptions regarding the actual motion pattern displayed by the snake robot.

B. Analysis of turning motion during lateral undulation

Having determined in the previous subsection how propulsion is generally achieved with a snake robot, we now investigate how a snake robot achieves turning motion. We assume that the robot moves according to the gait pattern lateral undulation.

As described in Section III, lateral undulation is achieved by controlling the joints of the snake robot according to (6). The simplest and most common approach for changing the direction of the motion during this gait pattern is to use the parameter ϕ_o in (6), which represents a joint angle offset. The reason why a non-zero ϕ_o induces rotational motion of a snake robot is illustrated in Fig. 4. In particular, the analysis presented in the previous subsection implies that the net propulsive ground friction forces produced by a link points in the direction about which the link angle oscillates. When $\phi_o = 0$, we see from the top of Fig. 4 that each link angle will oscillate about the forward direction of the robot. These oscillations produce propulsive forces which propel the robot forward along a straight line. When ϕ_o is
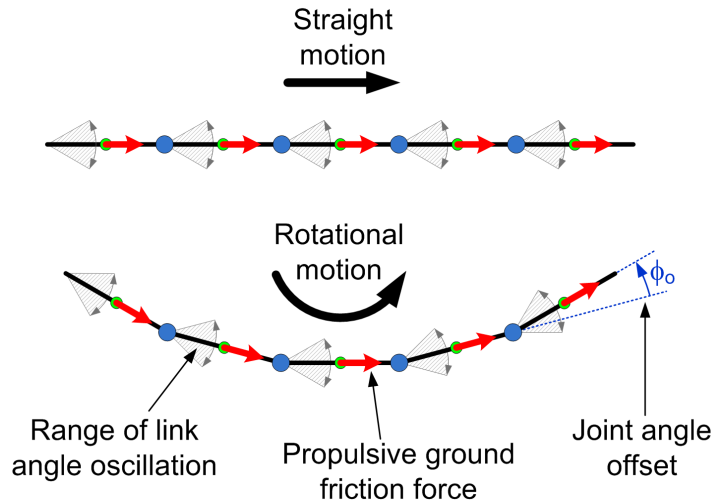
Fig. 4. The net propulsive ground friction forces produced by a link points in the direction about which the link angle oscillates. By offsetting the joint angles, the direction of the net propulsive forces on the links will point along an arc, thereby inducing rotational motion of the snake robot.

non-zero, on the other hand, we see from the bottom of Fig. 4 that the direction of the net propulsive forces on the links will point along an arc, thereby inducing rotational motion of the snake robot.

To further investigate how a joint angle offset influences the turning motion of a snake robot, we have simulated two trials of lateral undulation of a snake robot described by (5) with $N = 10$ links of length $l = 0.14$ m, and with friction coefficients $c_t = 1$ and $c_n = 10$. In the first trial, the snake robot was controlled according to (6) with $\alpha = 30°$, $\omega = 50°/_s$, and $\delta = 40°$. The offset angle was set to $\phi_o = 5°$ in the time interval $t \in [20, 30]$ and $\phi_o = -10°$ in the time interval $t \in [50, 60]$. The offset angle was $\phi_o = 0°$ outside these two time intervals. The parameters of the second trial were identical to the first trial except that we increased the frequency of the joint motion to $\omega = 80°/_s$ in order to increase the forward velocity. The trace of the head during the motion from the first and the second trial is shown in Fig. 5(a) and Fig. 5(b), respectively, while Fig. 5(c) shows the average joint angle during both trials, which is defined as $\overline{\phi} = \frac{1}{N-1} \sum_{i=1}^{N-1} \phi_i$. The triangles pointing up and down in Fig. 5(a)-(b) indicate, respectively, the beginning and end of the two time intervals where ϕ_o is non-zero.

Fig. 5 shows that the snake robot crawls forward without turning as long as the average joint angle, $\overline{\phi}$, is zero. However, when the average joint angle is non-zero, the direction of the motion changes. We see from the figure that a positive (resp. negative) average joint angle produces a counterclockwise (resp. clockwise) rotation of the snake robot. We also see that the rate of directional change is increased by
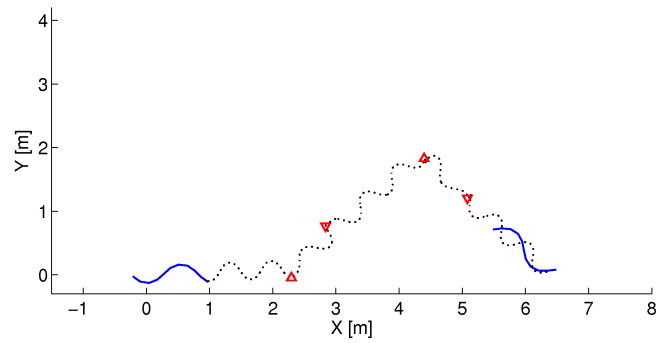
(a) Trace of the head of the snake robot at low forward velocity ($\omega = 50^\circ/_s$).
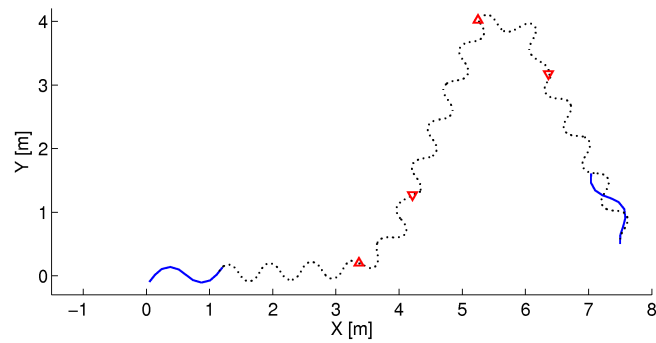
(b) Trace of the head of the snake robot at high forward velocity ($\omega = 80^\circ/_s$).
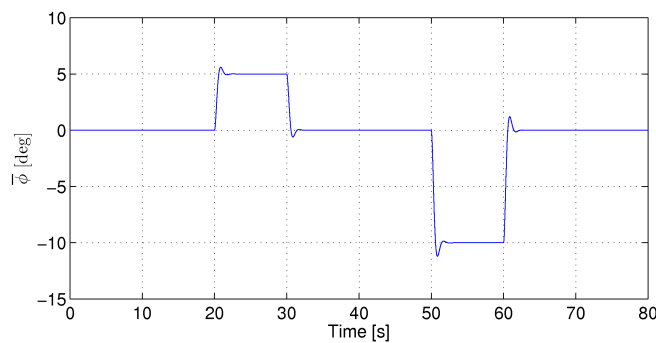
(c) The average joint angle during both trials.

Fig. 5.   Two simulated trials of lateral undulation of a snake robot with $N = 10$ links. In both trials, a joint angle offset of $\phi_o = 5^\circ$ and $\phi_o = -10^\circ$ is introduced at $t = 20$ s and $t = 50$ s, respectively.

increasing the amplitude of the average joint angle. This result is supported by the directional controllers for snake locomotion considered in e.g.[9;30]. Moreover, Fig. 5 also shows that the rate of directional change is larger in the second trial. Since the only difference between the two trials is that the forward velocity is larger in the second trial, we can conclude that the rate of directional change for some fixed joint angle offset is also increased by increasing the forward velocity of the snake robot.

The following property summarizes the above analysis:

Property 4: During *lateral undulation* with a snake robot described by (5) with $c_n > c_t$, the overall direction of the locomotion remains constant as long as the average joint angle is zero, but will change in the counterclockwise (resp. clockwise) direction when the average joint angle is positive (resp. negative). The rate of directional change of the locomotion is increased by increasing the amplitude of the average joint angle and/or by increasing the forward velocity (assuming that the average joint angle is non-zero).

Remark 5: Although Property 4 was developed under the assumption that the snake robot moves according to lateral undulation, we claim that the property also applies to other gait patterns. In particular, we claim that any gait pattern which propels a snake robot forward along a straight line will induce rotational motion of the robot if a non-zero joint angle offset is introduced at each joint.

C. Analysis of relative link motion during lateral undulation

From the results of the two previous subsections, it should be clear that planar snake locomotion consists of periodic body shape changes that generate external forces that propel the snake forward. These body shape changes can be characterized in terms of the joint angles $\phi_i = \theta_{i+1} - \theta_i$ defined in Section II-A. From Property 1, we know that the forward motion is induced by the motion of the links *normal* to the forward direction. This result led the authors to wonder if the body shape changes can be characterized in terms of the translational displacements of the links instead of the rotational joint motion. The motivation behind this idea is that translational motion is generally less complex to model than rotational motion. In particular, the model given by (5), which describes the rotational link motion of a snake robot, is quite complex.

To elaborate this idea further, the motion of a snake robot described by (5) with $N = 10$ links of length $l = 0.14$ m is shown in the top of Fig. 6. The robot conducts lateral undulation along the global x axis in accordance with (6) with $\alpha = 30°$, $\omega = 30°/_s$, $\delta = 40°$, and $\phi_o = 0°$. The two bottom plots in Fig. 6 show the relative displacement between the CM (center of mass) of two arbitrarily chosen links (links 4 and 5) in the global x and y direction, respectively. The plots indicate that, during lateral undulation, the relative displacement between the CM of two adjacent links along the forward direction of motion
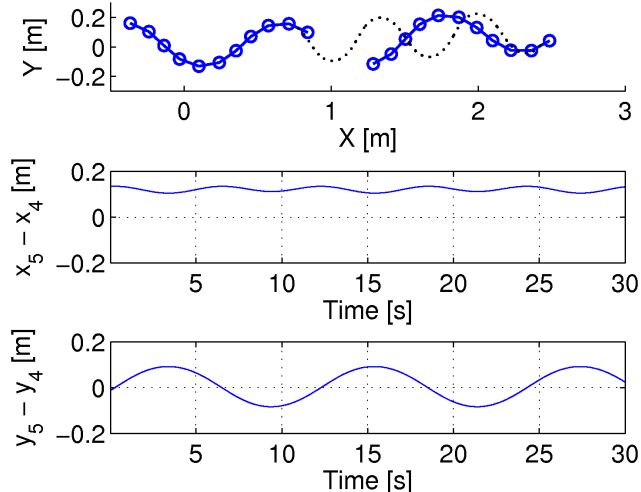
Fig. 6. Top: Simulated motion of a snake robot with $N = 10$ links. Middle: Relative displacement between the CM of link 4 and link 5 in the global x direction. Bottom: Relative displacement between the CM of link 4 and link 5 in the global y direction.

is approximately constant, while the relative displacement normal to the direction of motion oscillates around zero. This observation is an important basis for the modelling approach described in Section V and is summarized as follows:

Property 6: The change in body shape during lateral undulation consists mainly of relative displacements of the CM of the links *normal* to the forward direction of motion. The relative displacements of the CM of the links along the forward direction are approximately constant.

Remark 7: The relative link displacements *normal* to the direction of motion will *not* dominate over the relative link displacements *tangential* to the direction of motion when the amplitudes of the link angles become large. Property 6 is therefore valid only as long as the link angles are limited.

V. A SIMPLIFIED MODEL OF LATERAL UNDULATION

In this section, we employ the results from the previous section in order to develop a simplified model of a planar snake robot conducting lateral undulation. The model is intended for control design and stability analysis purposes.

A. Overview of the modelling approach

The idea behind the simplified model is illustrated in Fig. 7. The approach is basically to describe the body shape changes of a snake robot as *linear displacements* of the links with respect to each other
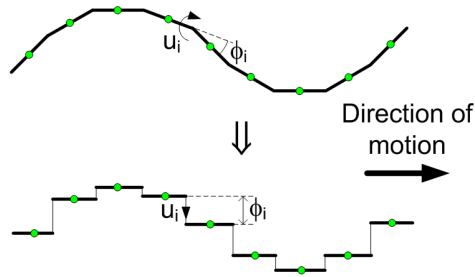
Fig. 7.   The revolute joints of the snake robot are modelled as prismatic joints that displace the CM of each link transversal to the direction of motion.

instead of rotational displacements. From Property 6, we know that these linear displacements should be normal to the forward direction of motion. In addition, we know from Property 1 that these transversal displacements of the links are what propel the snake robot forward. This essentially means that we will model the revolute joints of a snake robot as prismatic (translational) joints. The rotational motion of the links during body shape changes will in other words be disregarded. However, the model will still capture the *effect* of the rotational link motion during body shape changes, which we know from Property 6 to be primarily a linear displacement of the CM of the links normal to the forward direction of motion.

Remark 8: Property 1 makes no assumption regarding the gait pattern of the snake robot. Property 6, however, is only valid for gait patterns where the relative link displacements *normal* to the direction of motion dominate over the relative link displacements *tangential* to the direction of motion. The simplified model should therefore only be used to study gait patterns with *limited* link angles with respect to the forward direction. A discussion of the validity of the simplified model is provided in Section V-F.

Remark 9: We emphasize that the simplified model presented in this section is not intended as an accurate simulation model of snake robot locomotion. The model is intentionally based on several simplifying assumptions in order to arrive at equations of motion that are manageable for control design and stability analysis purposes. To this end, the model only needs to be *qualitatively* similar to the complex model presented in (5).

The kinematics and dynamics of the snake robot will be detailed in the following subsections in terms of the mathematical symbols described in Table II and illustrated in Fig. 8 and Fig. 9. We will consider a planar snake robot with N links of length l interconnected by $N - 1$ *prismatic* (translational) joints. All N links have the same mass m, and the total mass of the snake robot is thus Nm.
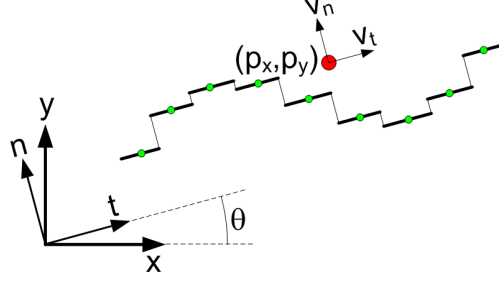
Fig. 8. Illustration of the two coordinate frames employed in the simplified model. The global x-y frame is fixed. The t-n frame is always aligned with the snake robot.
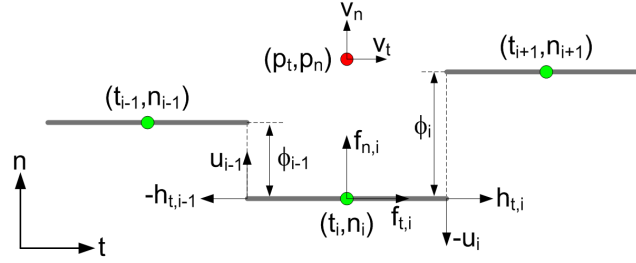

Fig. 9. Symbols characterizing the kinematics and dynamics of the snake robot.

The following vectors and matrices are used in the development of the model:

$$A = \begin{bmatrix} 1 & 1 & & \\ & . & . & \\ & & . & . \\ & & & 1 & 1 \end{bmatrix}, D = \begin{bmatrix} 1 & -1 & & \\ & . & . & \\ & & . & . \\ & & & 1 & -1 \end{bmatrix}$$

where $A \in \mathbb{R}^{(N-1) \times N}$ and $D \in \mathbb{R}^{(N-1) \times N}$. Furthermore,

$$e = \begin{bmatrix} 1 & . & . & 1 \end{bmatrix}^T \in \mathbb{R}^N, \quad \overline{e} = \begin{bmatrix} 1 & . & . & 1 \end{bmatrix}^T \in \mathbb{R}^{N-1},$$

$$\overline{D} = D^T \left(D D^T \right)^{-1} \in \mathbb{R}^{N \times (N-1)}.$$

The matrices A and D represent, respectively, an *addition* and a *difference* matrix, which will be used, respectively, for adding and subtracting pairs of adjacent elements of a vector. Furthermore, the vectors e and $\overline{e}$ represent summation vectors, which will be used for adding all elements of N-dimensional and $(N-1)$-dimensional vectors, respectively. The matrix $\overline{D}$ has been defined above since it appears several times during the development of the model. We will use subscript i to denote element i of a vector.

TABLE II

PARAMETERS THAT CHARACTERIZE THE SNAKE ROBOT.

Symbol	Description
N	Number of links.
l	Length of a link.
m	Mass of each link.
ϕ_i	Normal direction distance between links i and $i+1$.
$v_{\phi,i}$	Relative velocity between links i and $i+1$.
θ	Orientation of the snake robot.
v_θ	Angular velocity of the snake robot.
(t_i, n_i)	Coordinates of the CM of link i in the t-n frame.
(p_t, p_n)	Coordinates of the CM of the robot in the t-n frame.
(p_x, p_y)	Coordinates of the CM of the robot in the global frame.
(v_t, v_n)	Forward and normal direction velocity of the robot.
u_i	Actuator force at joint i.
$(f_{x,i}, f_{y,i})$	Friction force on link i in the global frame.
$(f_{t,i}, f_{n,i})$	Friction force on link i in the t-n frame.

When parameters of the snake robot links are assembled into a vector, we associate element i of this vector with link i.

B. The kinematics of the snake robot

The snake robot moves in the horizontal plane and has a total of $N+2$ degrees of freedom. We define the motion of the robot with respect to the two coordinate frames illustrated in Fig. 8. The x-y frame is the fixed global frame. The t-n frame is always aligned with the snake robot, i.e. the t and n axis always point in the *tangential* and *normal* direction of the robot, respectively. The origin of both frames are fixed and coincide. We will denote the direction of the t axis as the *tangential* or *forward* direction of the robot, and the direction of the n axis as the *normal* direction. Note that we do not refer to the t-n frame as the *body* frame of the snake robot since the t-n frame is not fixed to the robot. However, if a body frame fixed to the robot had been defined, the orientation of this frame would be identical to the orientation of the t-n frame.

The position of the snake robot is described through the coordinates of its CM (center of mass). As

seen in Fig. 8 and Fig. 9, the global frame position of the robot is denoted by $(p_x, p_y) \in \mathbb{R}^2$, while the t-n frame position is denoted by $(p_t, p_n) \in \mathbb{R}^2$. The global frame orientation of the robot is denoted by $\theta \in \mathbb{R}$ and is expressed with respect to the global x axis with counterclockwise positive direction. The angle between the global x axis and the t axis is also θ since the t-n frame is always aligned with the robot. Describing the position in a frame which is always aligned with the snake robot is inspired by and similar to a coordinate transformation proposed by Pettersen and Egeland[31].

Remark 10: There are many possible choices of orientation for a snake robot with revolute joints. In order to study lateral undulation, it is useful to employ a choice of orientation which is aligned with the forward direction of the snake robot. To this end, a common approach in previous literature has been to describe the orientation of a snake robot as the mean of the absolute link angles[16;15]. The simplified model proposed in this section provides a representation of orientation in terms of the scalar variable θ, which is always aligned with the forward direction of the snake robot.

The relationship between the t-n frame position and the global frame position is given by

$$p_t = p_x \cos\theta + p_y \sin\theta \tag{13a}$$

$$p_n = -p_x \sin\theta + p_y \cos\theta \tag{13b}$$

As illustrated in Fig. 8, the forward and normal direction velocity of the CM of the snake robot are denoted by $v_t \in \mathbb{R}$ and $v_n \in \mathbb{R}$, respectively. Using (1), the relationship between the global frame velocity of the robot and the t-n frame velocity is given by

$$\dot{p}_x = v_t \cos\theta - v_n \sin\theta \tag{14a}$$

$$\dot{p}_y = v_t \sin\theta + v_n \cos\theta \tag{14b}$$

and the inverse relationship is given by

$$v_t = \dot{p}_x \cos\theta + \dot{p}_y \sin\theta \tag{15a}$$

$$v_n = -\dot{p}_x \sin\theta + \dot{p}_y \cos\theta \tag{15b}$$

Differentiating (13) with respect to time and inserting (15) gives

$$\dot{p}_t = v_t + p_n \dot{\theta} \tag{16a}$$

$$\dot{p}_n = v_n - p_t \dot{\theta} \tag{16b}$$

We denote the t-n frame position of the CM of link i by $(t_i, n_i) \in \mathbb{R}^2$. The $N-1$ prismatic joints of the snake robot control the normal direction distance between the links. As seen in Fig. 9, the normal

direction distance between link i and link $i+1$ is given by

$$\phi_i = n_{i+1} - n_i \tag{17}$$

and represents the coordinate of joint i. The controlled distance ϕ_i replaces the controlled joint angle in the original model given by (5). The link positions are constrained by the prismatic joints according to

$$t_i - t_{i+1} + l = 0 \tag{18a}$$

$$n_i - n_{i+1} + \phi_i = 0 \tag{18b}$$

These holonomic constraints may be expressed in matrix form for all links as

$$\boldsymbol{D}\boldsymbol{t} + l\bar{\boldsymbol{e}} = 0 \tag{19a}$$

$$\boldsymbol{D}\boldsymbol{n} + \boldsymbol{\phi} = 0 \tag{19b}$$

where $\boldsymbol{D}$ and $\bar{\boldsymbol{e}}$ are defined in Section V-A, $\boldsymbol{t} = (t_1, \cdots, t_N) \in \mathbb{R}^N$, $\boldsymbol{n} = (n_1, \cdots, n_N) \in \mathbb{R}^N$, and $\boldsymbol{\phi} = (\phi_1, \cdots, \phi_{N-1}) \in \mathbb{R}^{N-1}$. The t-n frame position of the CM of the snake robot can be written in terms of the link positions as

$$p_t = \frac{1}{N}\boldsymbol{e}^T\boldsymbol{t} \tag{20a}$$

$$p_n = \frac{1}{N}\boldsymbol{e}^T\boldsymbol{n} \tag{20b}$$

where $\boldsymbol{e}$ is defined in Section V-A. Combining (19a), (19b), (20a) and (20b) gives

$$\begin{bmatrix} \boldsymbol{D} \\ \frac{1}{N}\boldsymbol{e}^T \end{bmatrix} \boldsymbol{t} = \begin{bmatrix} -l\bar{\boldsymbol{e}} \\ p_t \end{bmatrix}, \quad \begin{bmatrix} \boldsymbol{D} \\ \frac{1}{N}\boldsymbol{e}^T \end{bmatrix} \boldsymbol{n} = \begin{bmatrix} -\boldsymbol{\phi} \\ p_n \end{bmatrix} \tag{21}$$

We can solve (21) for the link positions as

$$\boldsymbol{t} = p_t\boldsymbol{e} - l\overline{\boldsymbol{D}}\bar{\boldsymbol{e}} \tag{22a}$$

$$\boldsymbol{n} = p_n\boldsymbol{e} - \overline{\boldsymbol{D}}\boldsymbol{\phi} \tag{22b}$$

where $\overline{\boldsymbol{D}} = \boldsymbol{D}^T \left(\boldsymbol{D}\boldsymbol{D}^T\right)^{-1} \in \mathbb{R}^{N \times (N-1)}$. By differentiating (22a) and (22b) with respect to time and inserting (16a) and (16b), the individual link velocities are given as

$$\dot{\boldsymbol{t}} = \left(v_t + p_n\dot{\theta}\right)\boldsymbol{e} \tag{23a}$$

$$\dot{\boldsymbol{n}} = \left(v_n - p_t\dot{\theta}\right)\boldsymbol{e} - \overline{\boldsymbol{D}}\dot{\boldsymbol{\phi}} \tag{23b}$$

C. The ground friction model

In order to derive the ground friction forces in the simplified model, we use the viscous ground friction model defined in (3) as a starting point. In particular, since the simplified model targets snake locomotion with limited link angles with respect to the forward direction (see Remark 8), we approximate the friction model in (3) under the assumption that the link angles are small.

Let us begin by considering a snake robot with revolute joints. When the robot is headed along the global positive x axis, the angle of link i with respect to the forward direction is given by θ_i. Moreover, when θ_i is small, the following approximations are valid:

$$\sin^2 \theta_i \approx 0 \tag{24}$$

$$\cos^2 \theta_i \approx 1 \tag{25}$$

$$\sin \theta_i \cos \theta_i \approx \theta_i \tag{26}$$

The approximation in (26) is illustrated in Fig. 10, where we see that $\sin \theta_i \cos \theta_i$ and θ_i are very close for $|\theta_i| < 20°$ (≈ 0.34 rad) and start to deviate as $|\theta_i|$ approaches $30°$ ($= 0.5$ rad). Inserting (24), (25), and (26) into the ground friction model (3) gives

$$\begin{bmatrix} f_{x,i} \\ f_{y,i} \end{bmatrix} = - \begin{bmatrix} c_t & (c_t - c_n)\,\theta_i \\ (c_t - c_n)\,\theta_i & c_n \end{bmatrix} \begin{bmatrix} \dot{x}_i \\ \dot{y}_i \end{bmatrix} \tag{27}$$

Since the snake robot is headed along the global x axis, the velocities $\dot{x}_i$ and $\dot{y}_i$ correspond to the velocity of link i in the tangential and normal direction of the snake robot, respectively, while the forces $f_{x,i}$ and $f_{y,i}$ correspond to the friction force on link i in the tangential and normal direction, respectively. By denoting the friction force components on link i in the t-n frame of the simplified model by $f_{t,i}$ and $f_{n,i}$, respectively, and remembering from Section V-B that the t-n frame velocity components of link i are given by $\dot{t}_i$ and $\dot{n}_i$, respectively, we therefore have that

$$\dot{x}_i = \dot{t}_i, \quad \dot{y}_i = \dot{n}_i \tag{28}$$

$$f_{x,i} = f_{t,i}, \quad f_{y,i} = f_{n,i} \tag{29}$$

What now remains before we can use the friction model in (27) in the simplified model of the snake robot is to write the link angle θ_i in terms of the simplified joint coordinates defined in (17). This is achieved with the approximation illustrated in Fig. 11. In particular, we estimate θ_i as the angle of the straight line from the CM of link $i - 1$ to the CM of link $i + 1$ with respect to the forward direction,
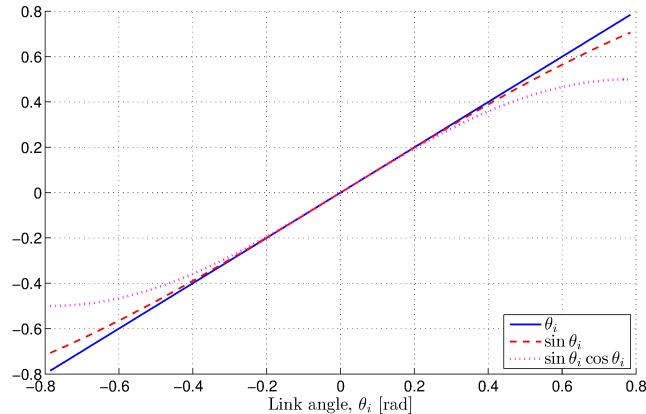
Fig. 10. Plots which show that the approximations $\sin \theta_i \approx \theta_i$ and $\sin \theta_i \cos \theta_i \approx \theta_i$ are valid for limited link angles.

which is denoted by θ_i^* in Fig. 11. We also see from Fig. 11 that the distance from the CM of link $i-1$ to the CM of link $i+1$ can be approximated as $2l$ when the link angles are limited. We can therefore estimate the angle of link i as

$$\theta_i \approx \sin \theta_i \approx \sin \theta_i^* \approx \frac{y_{i+1} - y_{i-1}}{2l} \tag{30}$$

The fact that $\sin \theta_i \approx \theta_i$ for limited link angles is shown in Fig. 10. Furthermore, since the joint coordinate ϕ_i of the simplified model corresponds to the normal direction distance between link i and link $i+1$, we have that

$$y_{i+1} - y_{i-1} = \phi_{i-1} + \phi_i \tag{31}$$

By inserting the identities in (28), (29), (30), and (31) into (27), we can write the viscous ground friction force on link i in the simplified model as

$$\begin{bmatrix} f_{t,i} \\ f_{n,i} \end{bmatrix} = \begin{bmatrix} -c_t & c_p\left(\phi_{i-1} + \phi_i\right) \\ c_p\left(\phi_{i-1} + \phi_i\right) & -c_n \end{bmatrix} \begin{bmatrix} \dot{t}_i \\ \dot{n}_i \end{bmatrix}_{\dot{\theta}=0} \tag{32}$$

where

$$c_p = \frac{c_n - c_t}{2l} \tag{33}$$

The parameter c_p is a propulsion coefficient (p is short for *propulsion*) which maps the normal direction link velocities and the joint coordinates into propulsive friction forces in the forward (tangential) direction of the snake robot. The subscript $\dot{\theta} = 0$ after the link velocity in (32) means that we choose to disregard the link velocity components due to the angular velocity $\dot{\theta}$ of the snake robot (we are now considering
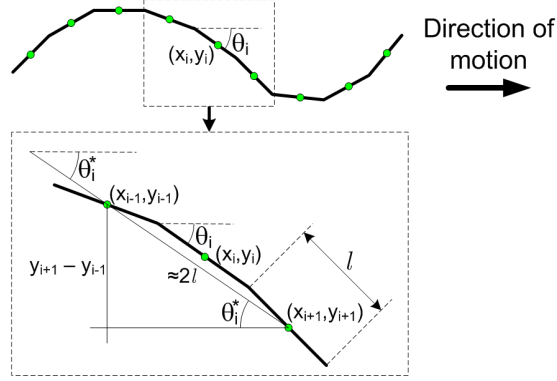
Fig. 11. The body angle of link i is θ_i for a snake robot with revolute joints. For a snake robot with prismatic joints, we approximate the body angle of link i based on the relative transversal distance to its two neighbouring links.

the simplified model of the snake robot, where θ denotes the orientation of the robot and not a link angle). Calculating $\dot{t}_i$ and $\dot{n}_i$ under the assumption that $\dot{\theta} = 0$ is a reasonable approximation since the dynamics of the angular rotation of the snake robot will generally be much slower than the body shape dynamics. This assumption also simplifies the ground friction model significantly.

The friction forces in (32) on all N links can now be written in matrix form as

$$\begin{bmatrix} \boldsymbol{f}_t \\ \boldsymbol{f}_n \end{bmatrix} = \begin{bmatrix} -c_t \boldsymbol{I}_N & c_p \operatorname{diag}\left(\boldsymbol{A}^T \boldsymbol{\phi}\right) \\ c_p \operatorname{diag}\left(\boldsymbol{A}^T \boldsymbol{\phi}\right) & -c_n \boldsymbol{I}_N \end{bmatrix} \begin{bmatrix} \dot{\boldsymbol{t}} \\ \dot{\boldsymbol{n}} \end{bmatrix}_{\dot{\theta}=0} \tag{34}$$

where $\boldsymbol{f}_t \in \mathbb{R}^N$ and $\boldsymbol{f}_n \in \mathbb{R}^N$ contain, respectively, the tangential and normal direction friction forces on the links, $\boldsymbol{I}_N$ is the $N \times N$ identity matrix, $\boldsymbol{A}$ is defined in Section V-A, and the operator $\operatorname{diag}(\cdot)$ produces a diagonal matrix with the elements of its argument along its diagonal. Inserting (23a) and (23b) into (34) with $\dot{\theta} = 0$ finally gives

$$\boldsymbol{f}_t = -c_t v_t \boldsymbol{e} + c_p \operatorname{diag}\left(\boldsymbol{A}^T \boldsymbol{\phi}\right)\left(v_n \boldsymbol{e} - \overline{\boldsymbol{D}}\dot{\boldsymbol{\phi}}\right) \tag{35a}$$

$$\boldsymbol{f}_n = -c_n v_n \boldsymbol{e} + c_n \overline{\boldsymbol{D}}\dot{\boldsymbol{\phi}} + c_p v_t \operatorname{diag}\left(\boldsymbol{A}^T \boldsymbol{\phi}\right) \boldsymbol{e} \tag{35b}$$

Note that a discussion related to the validity of the derived ground friction model is given in Section V-F.

D. The dynamics of the snake robot

In this section, we derive the model of the translational and rotational acceleration of the snake robot.

1) The translational dynamics of the snake robot: We use first principles to describe the translational dynamics. In particular, we can see from Fig. 9 that the force balance for link i is given by

$$m\ddot{t}_i = f_{t,i} + h_{t,i} - h_{t,i-1} \tag{36a}$$

$$m\ddot{n}_i = f_{n,i} - u_i + u_{i-1} \tag{36b}$$

where $f_{t,i}$ and $f_{n,i}$ are the ground friction forces defined in (32), $h_{t,i}$ and $-h_{t,i-1}$ are the joint constraint forces on link i from link $i+1$ and link $i-1$, respectively, and $-u_i$ and u_{i-1} are the actuator forces exerted on link i from link $i+1$ and link $i-1$, respectively. The joint constraint forces, $h_{t,i}$ and $-h_{t,i-1}$, prevent relative motion between the links in the tangential direction and the actuator forces, $-u_i$ and u_{i-1}, produce relative motion between the links in the normal direction. The force balance for all links can be written in matrix form as

$$m\ddot{\boldsymbol{t}} = \boldsymbol{f}_t + \boldsymbol{D}^T \boldsymbol{h}_t \tag{37a}$$

$$m\ddot{\boldsymbol{n}} = \boldsymbol{f}_n - \boldsymbol{D}^T \boldsymbol{u} \tag{37b}$$

where $\boldsymbol{D}$ is defined in Section V-A, $\boldsymbol{h}_t = (h_{t,1}, \cdots, h_{t,N-1}) \in \mathbb{R}^{N-1}$, and $\boldsymbol{u} = (u_1, \cdots, u_{N-1}) \in \mathbb{R}^{N-1}$. Premultiplying (37b) by $\frac{1}{m}\boldsymbol{D}$ gives

$$\boldsymbol{D}\ddot{\boldsymbol{n}} = \frac{1}{m}\boldsymbol{D}\boldsymbol{f}_n - \frac{1}{m}\boldsymbol{D}\boldsymbol{D}^T \boldsymbol{u} \tag{38}$$

By differentiating (19b) twice with respect to time, it is easily seen that $\boldsymbol{D}\ddot{\boldsymbol{n}} = -\ddot{\phi}$. We can therefore write the body shape dynamics of the snake robot as

$$\ddot{\phi} = -\frac{1}{m}\boldsymbol{D}\boldsymbol{f}_n + \frac{1}{m}\boldsymbol{D}\boldsymbol{D}^T \boldsymbol{u} \tag{39}$$

Inserting (35b) into (39) and using the easily verifiable relations $\boldsymbol{D}\boldsymbol{e} = \boldsymbol{0}$, $\boldsymbol{D}\overline{\boldsymbol{D}} = \boldsymbol{I}_{N-1}$, and $\boldsymbol{D}\operatorname{diag}\left(\boldsymbol{A}^T \phi\right)\boldsymbol{e} = -\boldsymbol{A}\boldsymbol{D}^T \phi$, we get

$$\ddot{\phi} = -\frac{c_n}{m}\dot{\phi} + \frac{c_p}{m}v_t \boldsymbol{A}\boldsymbol{D}^T \phi + \frac{1}{m}\boldsymbol{D}\boldsymbol{D}^T \boldsymbol{u} \tag{40}$$

The tangential and normal direction acceleration of the CM of the snake robot, denoted by $\dot{v}_t$ and $\dot{v}_n$, respectively, are given as the sum of all tangential and normal direction forces on the links divided by the mass of the snake robot, Nm. This is written

$$\dot{v}_t = \frac{1}{Nm}\left(\boldsymbol{e}^T m\ddot{\boldsymbol{t}}\right) = \frac{1}{Nm}\boldsymbol{e}^T \boldsymbol{f}_t \tag{41a}$$

$$\dot{v}_n = \frac{1}{Nm}\left(\boldsymbol{e}^T m\ddot{\boldsymbol{n}}\right) = \frac{1}{Nm}\boldsymbol{e}^T \boldsymbol{f}_n \tag{41b}$$

where we note that the joint constraint forces, $\boldsymbol{h}_t$, and the actuator forces, $\boldsymbol{u}$, are eliminated when the link accelerations are summed, i.e. $\boldsymbol{e}^T \boldsymbol{D}^T = \boldsymbol{0}$. Inserting (35a) and (35b) into (41a) and (41b), and using the easily verifiable relations $\boldsymbol{e}^T \operatorname{diag} \left(\boldsymbol{A}^T \boldsymbol{\phi} \right) \boldsymbol{e} = 2\overline{\boldsymbol{e}}^T \boldsymbol{\phi}$, $\boldsymbol{e}^T \overline{\boldsymbol{D}} = \boldsymbol{0}$, and $\boldsymbol{e}^T \operatorname{diag} \left(\boldsymbol{A}^T \boldsymbol{\phi} \right) \overline{\boldsymbol{D}} = \boldsymbol{\phi}^T \boldsymbol{A} \overline{\boldsymbol{D}}$, we get

$$\dot{v}_t = -\frac{c_t}{m} v_t + \frac{2c_p}{Nm} v_n \overline{\boldsymbol{e}}^T \boldsymbol{\phi} - \frac{c_p}{Nm} \boldsymbol{\phi}^T \boldsymbol{A} \overline{\boldsymbol{D}} \dot{\boldsymbol{\phi}} \tag{42a}$$

$$\dot{v}_n = -\frac{c_n}{m} v_n + \frac{2c_p}{Nm} v_t \overline{\boldsymbol{e}}^T \boldsymbol{\phi} \tag{42b}$$

2) The rotational dynamics of the snake robot: The translational motion of a snake robot with revolute joints is produced by the translational displacements of the links (see Property 1). The essence of the approach underlying the simplified model of the snake robot is therefore to disregard the rotational link motion and instead only consider the translational displacements of the links. The *rotational* motion of a snake robot, on the other hand, is determined by the orientation of the links. A drawback of disregarding the rotational link motion is therefore that we remove the primary cause of the rotational motion of the robot. For this reason, a pure first principles perspective on the rotational dynamics of a snake robot with *translational* joints (as considered in the simplified model) will *not* produce a model which resembles the rotational dynamics of a snake robot with *revolute* joints.

Instead of using first principles, we therefore choose to develop a simplified model of the rotational dynamics of the snake robot based on our *qualitative* understanding of how the rotational motion is produced. In particular, we will base the model on Property 4, which was derived in Section IV-B. This property states that the direction of the forward motion changes when the average of the joint angles is nonzero and that the rate of directional change is increased by increasing the average of the joint angles and/or by increasing the forward velocity (assuming that the average of the joint angles is non-zero). In the simplified model, the direction of the forward motion is given by the orientation θ, the forward velocity is given by v_t, and the average of the joint angles corresponds to the average of the joint coordinates, $\overline{\boldsymbol{e}}^T \boldsymbol{\phi} / (N-1)$. Property 4 therefore suggests that we can describe the overall torque that induces the rotational motion of a snake robot as

$$\ddot{\theta}_{\text{rotation}} = \lambda_2 v_t \frac{\overline{\boldsymbol{e}}^T \boldsymbol{\phi}}{N-1} \tag{43}$$

where λ_2 is some constant parameter which determines the scaling of the mapping from average joint coordinate and forward velocity to rotational acceleration. Furthermore, there must necessarily act ground friction forces on the snake robot which induce a ground friction torque that opposes the rotational motion. Since the ground friction forces are of viscous type, we also assume that the rotational friction torque is

viscous. We choose to model this viscous friction torque as

$$\ddot{\theta}_{\text{resistance}} = -\lambda_1 \dot{\theta} \tag{44}$$

where λ_1 is some constant parameter which determines the scaling of the mapping from rotational velocity to rotational acceleration. By combining (43) and (44), we can write the simplified model of the rotational dynamics of the snake robot as

$$\ddot{\theta} = -\lambda_1 \dot{\theta} + \frac{\lambda_2}{N-1} v_t \bar{e}^T \phi \tag{45}$$

Although the model of $\ddot{\theta}$ is not based on first principles, we conjecture that the behaviour of this model will be *qualitatively* similar to the behaviour of a snake robot with revolute joints, and also *quantitatively* similar when the parameters λ_1 and λ_2 are properly chosen. This claim is supported by the stabilizability and controllability analysis of the simplified model presented in Sections VI and VII, respectively, and by the simulation results presented in Section IX.

Remark 11: Note that the model in (45) is very general and does not specify how to set the parameters λ_1 and λ_2 as a function of the remaining parameters of the snake robot. We conjecture that λ_1 is influenced by the friction coefficient c_n since the forces that induce the rotational friction torque are likely to act normally to the snake robot. Moreover, since the induced rotation of the robot is tightly coupled with the induced forward propulsion, we conjecture that λ_2 is influenced by the propulsion coefficient c_p.

E. The complete simplified model of the snake robot

This section summarizes the complete model of a planar snake robot with N links of mass m. Since the snake robot has $N+2$ degrees of freedom, a state vector containing the generalized coordinates and velocities of the robot will have dimension $2N + 4$. We choose the state vector of the system as

$$\boldsymbol{x} = (\boldsymbol{\phi}, \theta, p_x, p_y, \boldsymbol{v}_\phi, v_\theta, v_t, v_n) \in \mathbb{R}^{2N+4} \tag{46}$$

where $\boldsymbol{\phi} \in \mathbb{R}^{N-1}$ are the joint coordinates, $\theta \in \mathbb{R}$ is the absolute orientation, $(p_x, p_y) \in \mathbb{R}^2$ is the global frame position of the CM, $\boldsymbol{v}_\phi = \dot{\boldsymbol{\phi}} \in \mathbb{R}^{N-1}$ are the joint velocities, $v_\theta = \dot{\theta} \in \mathbb{R}$ is the angular velocity, and $(v_t, v_n) \in \mathbb{R}^2$ is the tangential and normal direction velocity of the snake robot. From (14), (40),

(42), and (45), we can write the complete model of the snake robot as

$$\dot{\boldsymbol{\phi}} = \boldsymbol{v}_{\phi} \tag{47a}$$

$$\dot{\theta} = v_{\theta} \tag{47b}$$

$$\dot{p}_x = v_t \cos\theta - v_n \sin\theta \tag{47c}$$

$$\dot{p}_y = v_t \sin\theta + v_n \cos\theta \tag{47d}$$

$$\dot{\boldsymbol{v}}_{\phi} = -\frac{c_n}{m}\boldsymbol{v}_{\phi} + \frac{c_p}{m}v_t\boldsymbol{A}\boldsymbol{D}^T\boldsymbol{\phi} + \frac{1}{m}\boldsymbol{D}\boldsymbol{D}^T\boldsymbol{u} \tag{47e}$$

$$\dot{v}_{\theta} = -\lambda_1 v_{\theta} + \frac{\lambda_2}{N-1}v_t\bar{\boldsymbol{e}}^T\boldsymbol{\phi} \tag{47f}$$

$$\dot{v}_t = -\frac{c_t}{m}v_t + \frac{2c_p}{Nm}v_n\bar{\boldsymbol{e}}^T\boldsymbol{\phi} - \frac{c_p}{Nm}\boldsymbol{\phi}^T\boldsymbol{A}\overline{\boldsymbol{D}}\boldsymbol{v}_{\phi} \tag{47g}$$

$$\dot{v}_n = -\frac{c_n}{m}v_n + \frac{2c_p}{Nm}v_t\bar{\boldsymbol{e}}^T\boldsymbol{\phi} \tag{47h}$$

where $\boldsymbol{u} \in \mathbb{R}^{N-1}$ are the actuator forces at the joints, $\boldsymbol{A}$, $\boldsymbol{D}$, $\overline{\boldsymbol{D}}$, and $\bar{\boldsymbol{e}}$ are defined in Section V-A, c_t and c_n correspond, respectively, to the tangential and normal direction friction coefficient of the links in the complex model of the snake robot, c_p is the propulsion coefficient defined in (33), and λ_1 and λ_2 are positive scalar constants which characterize the rotational motion of the snake robot.

We will assume that the actuator forces are always set according to the linearizing control law

$$\boldsymbol{u} = m\left(\boldsymbol{D}\boldsymbol{D}^T\right)^{-1}\left(\overline{\boldsymbol{u}} + \frac{c_n}{m}\dot{\boldsymbol{\phi}} - \frac{c_p}{m}v_t\boldsymbol{A}\boldsymbol{D}^T\boldsymbol{\phi}\right) \tag{48}$$

where $\overline{\boldsymbol{u}} \in \mathbb{R}^{N-1}$ is a new set of control inputs. This control law transforms the joint dynamics (47e) into $\dot{\boldsymbol{v}}_{\phi} = \overline{\boldsymbol{u}}$, which is identical to the joint dynamics of the complex model given by (5a).

F. Discussion of the simplified model

In this section, we provided a discussion of limitations and accuracy issues related to the simplified model of the snake robot.

1) Applications of the simplified model: The simplified model in (47) is *not* intended as an accurate simulation model of snake robot locomotion. The model is intentionally based on several simplifying assumptions in order to arrive at equations of motion which are manageable for control design and stability analysis purposes. To this end, the model only needs to be *qualitatively* similar to the complex model presented in (5). This *qualitative* similarity is supported by the stabilizability and controllability analysis of the simplified model presented in Sections VI and VII, respectively. There is also a *quantitative* similarity between the complex and the simplified model under conditions which are discussed in the following.

2) Accuracy issues of the simplified kinematics: The essence of the simplified modelling approach is to describe the body shape changes of a snake robot as linear link displacements normal to the forward direction of motion (i.e. to disregard the rotational link motion). This approach is only valid for gait patterns where the relative link displacements *normal* to the direction of motion dominate over the relative link displacements *tangential* to the direction of motion. Since the relative tangential link displacements increase with increasing link angles, the simplified model should only be used to study gait patterns with limited link angles with respect to the forward direction.

Note that there is an extension issue inherent in the simplified kinematics of the snake robot. As illustrated in the top of Fig. 12, the body length of a snake robot in the complex model is constant and equal to

$$L_{\text{comp}} = Nl \tag{49}$$

where N is the number of links and l is the link length. In the simplified model, however, the relative distance between the prismatic joints in the tangential direction of the snake robot is assumed to be constant and equal to the link length l. This assumption causes the total body length of the snake robot to increase when the relative normal direction distances between the links are increased. As shown in the bottom of Fig. 12, we can approximate the body length of the snake robot in the simplified model as

$$L_{\text{simp}} = l + \sum_{i=1}^{N-1} \sqrt{l^2 + \phi_i^2} \tag{50}$$

We see that $L_{\text{simp}} = L_{\text{comp}}$ when the snake robot is lying straight, but that L_{simp} increases when the joint coordinates are increased. We conjecture that the effects of this extension issue will be minimal as long as the joint coordinates of the snake robot are limited.

3) Accuracy issues of the ground friction model: The assumptions made during the development of the ground friction model in (32) are all valid for limited link angles. Unfortunately, it is difficult to derive a precise bound for the range of link angles where the friction model is valid. However, Fig. 10 suggests that (32) relies on approximations which are valid for link angles limited by approximately $|\theta_i| < 20°$. It therefore seems reasonable to expect the ground friction model in (32) to be *quantitatively* similar to the friction model in (3) for link angles satisfying this approximate bound.

Although the *quantitative* discrepancy between the models in (32) and (3) increases with increasing link angles, the properties derived in Section IV-A regarding the qualitative behaviour of a snake robot allow us to argue that the friction model in (32) is *qualitatively* similar to the friction model in (3) also for large link angles. In particular, we can easily see from (32) that the propulsive ground friction

Body length of snake robot with revolute joints

Body length of snake robot with prismatic joints
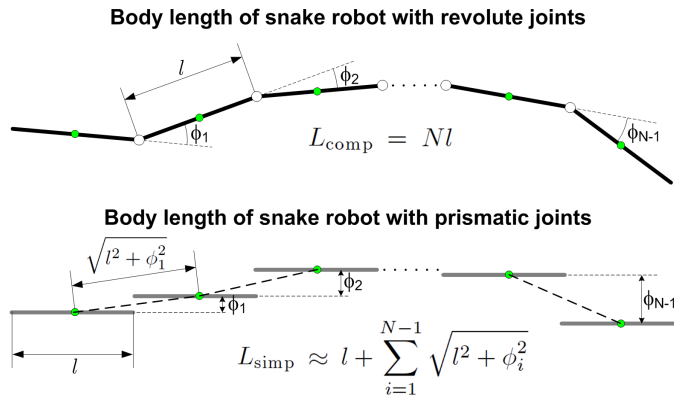
Fig. 12.   The body length of a snake robot with revolute joints (top) and of a snake robot with prismatic joints (bottom).

forces on link i that propel the robot forward are produced by the normal direction link velocity, $\dot{n}_i$. This is in direct accordance with Property 1. Furthermore, we see from (32) that the magnitude of the propulsive ground friction forces produced by link i is increased by increasing $|\phi_{i-1}+\phi_i|$, which, from (30) and (31), corresponds to increasing $|\theta_i|$. This is in direct accordance with Property 3. Finally, we can see from (32) that the forward direction friction force component produced by $\dot{n}_i$ is positive when $\mathrm{sgn}\,(\phi_{i-1}+\phi_i) = \mathrm{sgn}\,(\dot{n}_i)$ and negative otherwise, which is in direct accordance with Property 2. In summary, since the ground friction model in (32) directly captures the qualitative properties derived in Section IV-A, we argue that the friction model in (32) is *qualitatively* similar to the friction model in (3) also for large link angles.

Note that the *quantitative* discrepancy between the models in (32) and (3) will also increase when the ratio between the friction coefficients c_n and c_t is increased. In particular, the ground friction model in (32) is based on the approximation $c_t \cos^2 \theta_i + c_n \sin^2 \theta_i \approx c_t$, which is valid for small link angles. However, this approximation becomes less valid when the ratio c_n/c_t is increased.

4) Accuracy issues of the rotation dynamics: As explained in Section V-D2, the rotation dynamics of the snake robot in (45) was not derived from first principles. Instead, the model was developed to directly capture the *qualitative* behaviour of a snake robot during rotational motion. The rotation model in (45) is very general and does not specify how to set the parameters λ_1 and λ_2 as a function of the remaining parameters of the snake robot. However, we conjecture that the behaviour of this model will be *qualitatively* similar to the behaviour of a snake robot with revolute joints, and also *quantitatively* similar when the parameters λ_1 and λ_2 are properly chosen.

VI. STABILIZABILITY ANALYSIS OF THE SNAKE ROBOT

This section investigates the stabilizability properties of a snake robot described by the simplified model. While the results alone are interesting, the main purpose with the analysis is to show a fundamental similarity between the simplified and the complex model. This similarity is elaborated at the end of this section.

The analysis in this section proves a fundamental theorem concerning the properties of an asymptotically stabilizing control law for the snake robot to any equilibrium point $\boldsymbol{x}^e = (\boldsymbol{\phi}^e,\ \theta^e,\ p_x^e,\ p_y^e,\ \boldsymbol{v}_\phi = 0,\ v_\theta = 0,\ v_t = 0,\ v_n = 0)$. A well-known result by Brockett[32] states that a necessary condition for the existence of a *time-invariant* (i.e. not explicitly dependent on time) *continuous* state feedback law, $\boldsymbol{u} = \boldsymbol{u}\left(\boldsymbol{x}\right)$, that makes $\boldsymbol{x}^e$ asymptotically stable, is that the image of the mapping $(\boldsymbol{x}, \boldsymbol{u}) \mapsto \dot{\boldsymbol{x}}$ contains some neighbourhood of $\dot{\boldsymbol{x}} = \boldsymbol{0}$. A result by Coron and Rosier[33] states that a control system that can be asymptotically stabilized (in the Filippov sense[33]) by a *time-invariant discontinuous* state feedback law can be asymptotically stabilized by a *time-varying continuous* state feedback law. If, moreover, the control system is *affine* (i.e. linear with respect to the control input), then it can be asymptotically stabilized by a *time-invariant continuous* state feedback law. We now employ these results to prove the following fundamental result:

Proposition 12: An asymptotically stabilizing feedback control law for a planar snake robot described by (47) to any equilibrium point must be time-varying, i.e. of the form $\boldsymbol{u} = \boldsymbol{u}\left(\boldsymbol{x}, t\right)$.

Proof: The result by Brockett[32] states that the mapping $(\boldsymbol{x}, \boldsymbol{u}) \mapsto \dot{\boldsymbol{x}}$ must map an arbitrary neighbourhood of $\boldsymbol{x}^e$ onto a neighbourhood of $\dot{\boldsymbol{x}} = \boldsymbol{0}$. For this to be true, points of the form $\dot{\boldsymbol{x}} = (\dot{\boldsymbol{\phi}} = \boldsymbol{0},\ \dot{\theta} = 0,\ \dot{p}_x = 0,\ \dot{p}_y = 0,\ \dot{\boldsymbol{v}}_\phi = \boldsymbol{0},\ \dot{v}_\theta = 0,\ \dot{v}_t = \epsilon,\ \dot{v}_n = 0)$ must be contained in this mapping for some arbitrary $\epsilon \neq 0$ because points of this form are contained in every neighbourhood of $\dot{\boldsymbol{x}} = \boldsymbol{0}$. However, these points do not exist for the model (47) because $\dot{v}_t = 0 \neq \epsilon$ when all the other derivatives of the state vector are zero. Hence, the snake robot *cannot* be asymptotically stabilized to $\boldsymbol{x}^e$ by a *time-invariant continuous* state feedback law. Moreover, since the model is affine and *cannot* be asymptotically stabilized by a *time-invariant continuous* state feedback law, the result by Coron and Rosier[33] proves that the system can neither be asymptotically stabilized by a *time-invariant discontinuous* state feedback law. We can therefore conclude that an asymptotically stabilizing control law for the snake robot to any equilibrium point must be time-varying, i.e. of the form $\boldsymbol{u} = \boldsymbol{u}\left(\boldsymbol{x}, t\right)$. ∎

Remark 13: The authors have previously presented a similar stabilizability analysis[17] that considered a snake robot modelled by the complex model (5). This analysis produced an identical result as in

Proposition 12.

VII. Controllability analysis of the snake robot

This section investigates the controllability properties of a snake robot described by the simplified model. As for the previous section, our main intention is to show a fundamental similarity between the simplified and the complex model. This similarity is elaborated at the end of this section.

A. Controllability of the linearized system

We assume that the joint dynamics has been linearized by the control law (48) so that $\dot{\boldsymbol{v}}_\phi = \overline{\boldsymbol{u}}$. This enables us to rewrite the model of the snake robot (47) in the standard form of a control affine system as

$$\dot{\boldsymbol{x}} = \boldsymbol{f}(\boldsymbol{x}) + \sum_{j=1}^{N-1} \boldsymbol{g}_j \overline{u}_j \tag{51}$$

where $\boldsymbol{f}(\boldsymbol{x})$ contains all the terms from (47) with $\overline{\boldsymbol{u}} = \boldsymbol{0}_{(N-1)\times 1}$, $\overline{u}_j$ is the jth element of the control input vector $\overline{\boldsymbol{u}} \in \mathbb{R}^{N-1}$, and

$$\boldsymbol{g}_j = \begin{bmatrix} \boldsymbol{0}_{(N+2)\times 1} \\ \boldsymbol{e}_j \\ \boldsymbol{0}_{3\times 1} \end{bmatrix} \tag{52}$$

where $\boldsymbol{e}_j$ denotes the jth standard basis vector in $\mathbb{R}^{N-1}$ (the jth column of $\boldsymbol{I}_{N-1}$). The linearization of the model (51) about an equilibrium point $\boldsymbol{x}^e$ can be written as

$$\dot{\boldsymbol{z}} = \mathcal{A}\boldsymbol{z} + \mathcal{B}\overline{\boldsymbol{u}} \tag{53}$$

where $\boldsymbol{z} = \boldsymbol{x} - \boldsymbol{x}^e$, $\mathcal{A} = \left.\frac{\partial \boldsymbol{f}(\boldsymbol{x})}{\partial \boldsymbol{x}}\right|_{\boldsymbol{x}^e} \in \mathbb{R}^{(2N+4)\times(2N+4)}$, and $\mathcal{B} = \begin{bmatrix} \boldsymbol{g}_1 & \cdots & \boldsymbol{g}_{N-1} \end{bmatrix} \in \mathbb{R}^{(2N+4)\times(N-1)}$. The controllability matrix of the linearized system is given by $\boldsymbol{R} = \begin{bmatrix} \mathcal{B} & \mathcal{A}\mathcal{B} & \mathcal{A}^2\mathcal{B} & \cdots & \mathcal{A}^{2N+3}\mathcal{B} \end{bmatrix}$ and does *not* have full rank since it can be verified that $\text{rank}(\boldsymbol{R}) = 2N + 1$. The linearized model of the snake robot is therefore not controllable since the *Kalman rank condition*[34] is not satisfied. To study the controllability of the snake robot, we must therefore consider nonlinear controllability concepts.

B. Controllability of the nonlinear system

In the following, we will investigate the controllability of the snake robot in terms of *strong accessibility*[34] and *small-time local controllability* (STLC)[35]. *Strong accessibility* means that the dimension of the space that the system can reach in *exactly* time T for any $T > 0$ is equal to the dimension of the state space. Accessibility does *not* imply controllability, but is a necessary (although not sufficient) condition

for *small-time local controllability* (STLC). STLC is a stronger property than controllability and implies that the control input can steer the system in any direction in an arbitrarily small amount of time. For second-order systems, STLC is only possible from equilibrium states.

We assume that the snake robot consists of $N = 4$ links interconnected by $N - 1 = 3$ joints. The model of this robot will have $2N + 4 = 12$ states. We argue that the following controllability results will also be valid for a snake robot with more links. In particular, a snake robot with $N > 4$ links can behave as a snake robot with $N = 4$ links by fixing $(N - 4)$ joint coordinates at zero and allowing the remaining joints to move. By calculating Lie brackets of the system vector fields in (51), we can construct the following *accessibility algebra*[34] of the system evaluated at an equilibrium point $\boldsymbol{x}^e$:

$$\boldsymbol{\Delta}\left(\boldsymbol{x}^e\right) = \begin{bmatrix} \boldsymbol{\Delta}_1 & \cdots & \boldsymbol{\Delta}_{15} \end{bmatrix}_{\boldsymbol{x}^e} \in \mathbb{R}^{12 \times 15} \tag{54}$$

where

$$\boldsymbol{\Delta}_1 = \boldsymbol{g}_1, \boldsymbol{\Delta}_2 = \boldsymbol{g}_2, \boldsymbol{\Delta}_3 = \boldsymbol{g}_3,$$

$$\boldsymbol{\Delta}_4 = [\boldsymbol{f}, \boldsymbol{g}_1], \boldsymbol{\Delta}_5 = [\boldsymbol{f}, \boldsymbol{g}_2], \boldsymbol{\Delta}_6 = [\boldsymbol{f}, \boldsymbol{g}_3],$$

$$\boldsymbol{\Delta}_7 = [\boldsymbol{f}, [\boldsymbol{f}, \boldsymbol{g}_1]], \boldsymbol{\Delta}_8 = [\boldsymbol{f}, [\boldsymbol{f}, [\boldsymbol{f}, \boldsymbol{g}_1]]],$$

$$\boldsymbol{\Delta}_9 = [\boldsymbol{f}, [\boldsymbol{f}, [\boldsymbol{f}, [\boldsymbol{f}, \boldsymbol{g}_1]]]],$$

$$\boldsymbol{\Delta}_{10} = [\boldsymbol{g}_1, [\boldsymbol{f}, [\boldsymbol{f}, \boldsymbol{g}_2]]],$$

$$\boldsymbol{\Delta}_{11} = [\boldsymbol{g}_1, [\boldsymbol{f}, [\boldsymbol{f}, [\boldsymbol{f}, \boldsymbol{g}_2]]]],$$

$$\boldsymbol{\Delta}_{12} = [\boldsymbol{g}_1, [\boldsymbol{f}, [\boldsymbol{f}, [\boldsymbol{f}, [\boldsymbol{f}, \boldsymbol{g}_2]]]]],$$

$$\boldsymbol{\Delta}_{13} = [\boldsymbol{g}_1, [\boldsymbol{f}, [\boldsymbol{f}, [\boldsymbol{f}, [\boldsymbol{f}, [\boldsymbol{f}, \boldsymbol{g}_2]]]]]],$$

$$\boldsymbol{\Delta}_{14} = [\boldsymbol{g}_1, [\boldsymbol{f}, [\boldsymbol{f}, [\boldsymbol{f}, [\boldsymbol{f}, [\boldsymbol{f}, \boldsymbol{g}_3]]]]]],$$

$$\boldsymbol{\Delta}_{15} = [\boldsymbol{g}_2, [\boldsymbol{f}, [\boldsymbol{f}, [\boldsymbol{f}, [\boldsymbol{f}, [\boldsymbol{f}, \boldsymbol{g}_3]]]]]].$$

The accessibility algebra satisfies the following property:

Property 14: The accessibility algebra, $\boldsymbol{\Delta}\left(\boldsymbol{x}^e\right)$, has full rank ($\mathrm{rank}\left(\boldsymbol{\Delta}\left(\boldsymbol{x}^e\right)\right) = 12$) as long as the sum of the joint coordinates is nonzero, i.e. as long as $\bar{\boldsymbol{e}}^T \boldsymbol{\phi} \neq 0$.

Due to space constraints, we cannot present the expressions contained in each column of $\boldsymbol{\Delta}\left(\boldsymbol{x}^e\right)$. However, Property 14 can be shown to hold by employing a computer software for symbolic mathematics, such as *Matlab Symbolic Toolbox*. Note that we have included three more columns than rows in $\boldsymbol{\Delta}\left(\boldsymbol{x}^e\right)$ because different pairs of columns become linearly independent at certain configurations. Including three redundant columns ensures that $\boldsymbol{\Delta}\left(\boldsymbol{x}^e\right)$ does not drop rank at these configurations. We are now ready to state the following result:

Proposition 15: A planar snake robot described by (47) with $N = 4$ links is *locally strongly accessible* from any equilibrium point x^e satisfying $\bar{e}^T \phi \neq 0$.

Proof: The system is locally strongly accessible from x^e if the accessibility algebra of the system evaluated at x^e has full rank and does not contain the drift vector field f by itself (i.e. unbracketed)[34]. By Property 14, the snake robot satisfies these conditions as long as $\bar{e}^T \phi \neq 0$. This completes the proof. ∎

We now show that the snake robot does *not* satisfy sufficient conditions for *small-time local controllability* (STLC). STLC requires that we classify the Lie brackets of the system vector fields in terms of *good* and *bad* brackets. A Lie bracket is said to be *bad* if it contains the drift vector field f an odd number of times and each control vector field g_j an even number of times (0 is even). This classification is motivated by the fact that a bad bracket *may* have directional constraints. E.g. the drift vector f is *bad* because it only allows motion in its positive direction. The snake robot is STLC from an equilibrium point x^e if it is accessible from x^e and all *bad* brackets of the system can be neutralized, i.e. written as linear combinations of *good* brackets of lower θ-degree[35] or lower l-degree[36]. The model of the snake robot satisfies the following property:

Property 16: The brackets g_j, $[f, g_j]$, $[g_j, [f, g_k]]$, $[g_j, [f, [f, g_k]]]$, $[[f, g_j], [f, g_k]]$, $[f, [f, g_j]]$, $[f, [f, [f, g_j]]]$, $\cdots$, $[f, [\cdots [f, g_j]] \cdots]$, where $j, k \in \{1, 2, 3\}$ and $j \neq k$, are all *good* brackets, but does *not* span the entire 12-dimensional state space.

Due to space constraints, we are again unable to present the expressions contained in the brackets in Property 16. However, the property can be shown to hold by employing a computer software for symbolic mathematics, such as *Matlab Symbolic Toolbox*. Property 16 enables us to state the following result:

Proposition 17: A planar snake robot described by (47) with $N = 4$ links does *not* satisfy the sufficient conditions for *small-time local controllability* (STLC) presented by Sussmann[35] and by Bianchini and Stefani[36].

Proof: The bracket $[g_j, [f, [f, [f, g_j]]]]$ of the system, where $j \in \{1, 2, 3\}$, is a *bad* bracket. The only *good* brackets of lower θ-degree or lower l-degree that can neutralize this bad bracket are of the form g_j, $[f, g_j]$, $[g_j, [f, g_k]]$, $[g_j, [f, [f, g_k]]]$, $[[f, g_j], [f, g_k]]$, $[f, [f, g_j]]$, $[f, [f, [f, g_j]]]$, $\cdots$, $[f, [\cdots [f, g_j]] \cdots]$, where $j, k \in \{1, 2, 3\}$ and $j \neq k$. By Property 16, these brackets do *not* span the entire 12-dimensional state space. We therefore cannot express the bad bracket as a linear combination of good brackets of lower θ-degree or lower l-degree. Since there are bad brackets of the system that cannot be neutralized, the system does not satisfy the conditions for STLC presented by Sussmann[35] and by Bianchini and Stefani[36]. ∎

Remark 18: The authors have previously presented a similar controllability analysis[17] that considered a snake robot with $N = 4$ links modelled by the complex model (5). This analysis produced an identical result concerning STLC, but showed that the accessibility algebra of the system has full rank except for configurations where all joint coordinates are equal ($\phi_1 = \phi_2 = ... = \phi_{N-1}$), which will be the case when the snake robot is lying straight or forming an arc. The condition $\bar{e}^T\phi \neq 0$ stated in Proposition 15 states that a configuration is singular when the sum of the relative linear link displacements is zero. Since the sum of the relative linear link displacements is zero for both straight and arc shaped snake robots with revolute joints, the singular configurations of the complex model[17] are actually contained in the singular configurations stated in Proposition 15. This similarity supports the conjecture that the simplified model proposed in this paper captures the essential part of the dynamics of planar snake locomotion. Note that there are singular configurations of the simplified model that do not easily translate to the complex model. A wave shape where the sum of the relative linear link displacements is zero is a singular configuration in the simplified model, but is not singular to a snake robot with revolute joints. These additional singular configurations of the simplified model arise since the sum of the joint coordinates is employed to model the rotation of the snake in accordance with Property 4 in Section IV-B. Nonetheless, the most important conclusion to be drawn from Proposition 15 is that the snake robot is locally strongly accessible from *almost* any equilibrium point, except for certain singular configurations. This conclusion is in accordance with the previous results by the authors[17].

VIII. ANALYSIS OF THE VELOCITY DYNAMICS BASED ON AVERAGING THEORY

In this section, we will derive and investigate important properties of the velocity dynamics of a snake robot during lateral undulation. The analysis is based on *averaging theory*[37] since we are primarily interested in the overall speed and direction of the locomotion. The periodic fluctuations about the average trajectory of the snake is not of particular interest in this study.

A. Introduction to averaging theory

Consider a system of the form

$$\dot{x} = \varepsilon f(t, x) \tag{55}$$

where ε is a small positive parameter characterizing the magnitude of the perturbations of the system and $f(t, x)$ is T-periodic, i.e. $f(t + T, x) = f(t, x)$. A system that, in 'average', behaves similarly to the system in (55) is given by

$$\dot{x} = \varepsilon f_{av}(x) \tag{56}$$

where

$$\boldsymbol{f}_{av}(\boldsymbol{x}) = \frac{1}{T} \int\limits_{0}^{T} \boldsymbol{f}(\tau, \boldsymbol{x}) \mathrm{d}\tau \tag{57}$$

Note that the above integral should be calculated by treating the elements of the state vector $\boldsymbol{x}$ as constants. The smallness requirement on ε ensures that $\boldsymbol{x}$ varies slowly with t relative to the periodic excitation of the system. The system response will thereby be determined predominantly by the average of the excitation. The following theorem follows directly from Theorem 10.4 in a book by Khalil[29]:

Theorem 19: Let $\boldsymbol{f}(t, \boldsymbol{x})$ and its partial derivatives with respect to $\boldsymbol{x}$ be continuous and bounded for $(t, \boldsymbol{x}) \in [0, \infty) \times \mathbb{R}^n$. Suppose $\boldsymbol{f}$ is T-periodic in t for some $T > 0$ and ε is a positive parameter. Let $\boldsymbol{x}(t, \varepsilon)$ and $\boldsymbol{x}_{av}(t, \varepsilon)$ denote the solutions of (55) and (56), respectively. If the average system (56) has a *globally exponentially stable* equilibrium point and $\|\boldsymbol{x}(0, \varepsilon) - \boldsymbol{x}_{av}(0, \varepsilon)\| \leq k_0 \varepsilon$ for some $k_0 > 0$, then there exist $k > 0$ and $\varepsilon^* > 0$ such that for all $0 < \varepsilon < \varepsilon^*$,

$$\|\boldsymbol{x}(t, \varepsilon) - \boldsymbol{x}_{av}(t, \varepsilon)\| \leq k\varepsilon \quad \text{for all } t \in [0, \infty) \tag{58}$$

This theorem basically says that, for sufficiently small ε, the solutions of the original system (55) and the average system (56) remain close (of order ε) for all time if the initial conditions of the systems are close and the average system is *globally exponentially stable*. This implies that the original system will remain close to a trajectory which converges exponentially to the equilibrium point.

B. Model of the velocity dynamics of the snake robot

We will now study the velocity dynamics of the snake robot during lateral undulation (the gait pattern defined in (6)). The velocity dynamics is defined by (47f), (47g), and (47h), which give the dynamics of the forward direction velocity v_t, the normal direction velocity v_n, and the angular velocity v_θ of the snake robot. It was shown in Section III that we can achieve exponentially stable tracking of the joint reference coordinates (6) with the control law (9). We will therefore assume that $\boldsymbol{\phi}$ and $\boldsymbol{v}_\phi = \dot{\boldsymbol{\phi}}$ are given by (6) and (7), respectively. Furthermore, in order to arrive at a model of the velocity dynamics which is in the standard averaging form (55), we assume that the amplitude α and frequency ω of the joint motion are always set according to the rule

$$\omega = \frac{k_{\alpha\omega}}{\alpha^2} \tag{59}$$

where $k_{\alpha\omega} > 0$ is a controller parameter. Note that α and ω are still independent parameters since any choice of α and ω can be obtained by choosing $k_{\alpha\omega} = \alpha^2 \omega$. Using (6), (7), and (59), and introducing

the velocity state vector $\boldsymbol{v} = (v_t, v_n, v_\theta) \in \mathbb{R}^3$, the velocity dynamics can be written as

$$\dot{\boldsymbol{v}} = \begin{bmatrix} \dot{v}_t \\ \dot{v}_n \\ \dot{v}_\theta \end{bmatrix} = \boldsymbol{f}(t, \boldsymbol{v}) \tag{60}$$

where

$$\boldsymbol{f}(t, \boldsymbol{v}) = \begin{bmatrix} -\frac{c_t}{m} v_t + \frac{2c_p}{Nm} v_n f_1(\omega t) - \frac{c_p}{Nm} f_2(\omega t) \\ -\frac{c_n}{m} v_n + \frac{2c_p}{Nm} v_t f_1(\omega t) \\ -\lambda_1 v_\theta + \frac{\lambda_2}{N-1} v_t f_1(\omega t) \end{bmatrix} \tag{61}$$

$$f_1(\omega t) = (N-1)\phi_o + \sum_{i=1}^{N-1} \alpha \sin\left(\omega t + (i-1)\delta\right) \tag{62}$$

$$f_2(\omega t) = \sum_{i=1}^{N-1}\sum_{j=1}^{N-1} \left[\frac{k_{\alpha\omega}}{\alpha} \phi_o a_{ij} \cos\left(\omega t + (j-1)\delta\right) \right.$$
$$\left. + k_{\alpha\omega} a_{ij} \sin\left(\omega t + (i-1)\delta\right) \cos\left(\omega t + (j-1)\delta\right) \right] \tag{63}$$

and a_{ij} denotes element ij of the matrix $\boldsymbol{A}\overline{\boldsymbol{D}}$. To transform the model (60) into the standard form of averaging (55), we change the time scale from t to $\tau = \omega t$ and define $\varepsilon = 1/\omega$. Since $\frac{\mathrm{d}}{\mathrm{d}t} = \frac{1}{\varepsilon}\frac{\mathrm{d}}{\mathrm{d}\tau}$, the model (60) can now be written as

$$\frac{\mathrm{d}\boldsymbol{v}}{\mathrm{d}\tau} = \varepsilon \boldsymbol{f}(\tau, \boldsymbol{v}) \tag{64}$$

where

$$\boldsymbol{f}(\tau, \boldsymbol{v}) = \begin{bmatrix} -\frac{c_t}{m} v_t + \frac{2c_p}{Nm} v_n f_1(\tau) - \frac{c_p}{Nm} f_2(\tau) \\ -\frac{c_n}{m} v_n + \frac{2c_p}{Nm} v_t f_1(\tau) \\ -\lambda_1 v_\theta + \frac{\lambda_2}{N-1} v_t f_1(\tau) \end{bmatrix} \tag{65}$$

This model is in the standard form defined in (55). Note that when we require ε to be small, we equivalently require that $\omega = 1/\varepsilon$ is large.

C. Averaged model of the velocity dynamics

The averaged model of (64) is calculated in accordance with (56) as

$$\frac{\mathrm{d}\boldsymbol{v}}{\mathrm{d}\tau} = \varepsilon \frac{1}{2\pi} \int_0^{2\pi} \boldsymbol{f}(\tau, \boldsymbol{v})\mathrm{d}\tau \tag{66}$$

It can be verified that

$$\frac{1}{2\pi} \int_0^{2\pi} f_1(\tau)\mathrm{d}\tau = (N-1)\phi_o \tag{67}$$

$$\frac{1}{2\pi} \int\limits_{0}^{2\pi} f_2(\tau) \mathrm{d}\tau = -\frac{1}{2} k_{\alpha\omega} k_\delta \tag{68}$$

where the constant $k_\delta \in \mathbb{R}$ is defined as

$$k_\delta = \sum_{i=1}^{N-1} \sum_{j=1}^{N-1} a_{ij} \sin\left((j-i)\,\delta\right) \tag{69}$$

The averaged model can therefore be written as

$$\frac{\mathrm{d}\boldsymbol{v}}{\mathrm{d}\tau} = \varepsilon \left(\mathcal{A}\boldsymbol{v} + \boldsymbol{b}\right) \tag{70}$$

where

$$\mathcal{A} = \mathcal{A}\left(\phi_o\right) = \begin{bmatrix} -\frac{c_t}{m} & \frac{2(N-1)}{Nm} c_p \phi_o & 0 \\ \frac{2(N-1)}{Nm} c_p \phi_o & -\frac{c_n}{m} & 0 \\ \lambda_2 \phi_o & 0 & -\lambda_1 \end{bmatrix} \tag{71}$$

$$\boldsymbol{b} = \boldsymbol{b}\left(\alpha, \omega, \delta\right) = \begin{bmatrix} \frac{c_p}{2Nm} k_{\alpha\omega} k_\delta \\ 0 \\ 0 \end{bmatrix} \tag{72}$$

By changing time scale back to t using that $\frac{\mathrm{d}}{\mathrm{d}\tau} = \varepsilon \frac{\mathrm{d}}{\mathrm{d}t}$, the averaged model is given by

$$\dot{\boldsymbol{v}} = \mathcal{A}\boldsymbol{v} + \boldsymbol{b} \tag{73}$$

We see that the averaged model of the velocity dynamics is a linear system characterized by the parameters of the joint reference coordinates, i.e. by α, ω, δ, and ϕ_o.

Remark 20: The term *average velocity* will hereafter be used to denote the velocity described by the averaged model (73). This average velocity evolves according to the average changes of the original model (60) and will typically correspond to the average of the velocities of the original model over the last cycle of the periodic gait pattern (i.e. the last T seconds). The average velocity can, in other words, be regarded as a low-pass filtered version of the original velocity.

D. Stability analysis of the velocity dynamics

Before we determine the stability properties of the averaged model (73), we remove the constant offset term $\boldsymbol{b}$ with the coordinate transformation $\boldsymbol{z} = \boldsymbol{v} + \mathcal{A}^{-1}\boldsymbol{b}$. This gives

$$\dot{\boldsymbol{z}} = \dot{\boldsymbol{v}} = \mathcal{A}\left(\boldsymbol{z} - \mathcal{A}^{-1}\boldsymbol{b}\right) + \boldsymbol{b} = \mathcal{A}\boldsymbol{z} \tag{74}$$

It can be shown that the eigenvalues of $\mathcal{A}$ are given by

$$\text{eig}\left(\mathcal{A}\right) = \begin{bmatrix} -\frac{c_t+c_n}{2m} - \frac{\sqrt{(c_nN-c_tN)^2+(4(N-1)c_p\phi_o)^2}}{2Nm} \\ -\frac{c_t+c_n}{2m} + \frac{\sqrt{(c_nN-c_tN)^2+(4(N-1)c_p\phi_o)^2}}{2Nm} \\ -\lambda_1 \end{bmatrix} \tag{75}$$

The equilibrium point $z = 0$ is *globally exponentially stable* if all eigenvalues of $\mathcal{A}$ are negative[29], which can easily be verified to be the case if

$$|\phi_o| < \frac{N}{2\left(N-1\right)}\sqrt{c_tc_n} \tag{76}$$

The limit in (76) concerns the amplitude of the joint coordinate offset ϕ_o and is a function of the friction coefficients c_t and c_n. This limit is not relevant to a snake robot with revolute joints since the normal direction distance between the links of such mechanisms is physically constrained by the revolute joints. The instability issue in (76) therefore suggests that the approach of modelling the link motion as translational displacements breaks down when the displacements become large.

Assuming that we choose ϕ_o to satisfy the limit (76), then z will converge exponentially to zero, which means that v will converge exponentially to $-\mathcal{A}^{-1}b$, which means that the average velocity will converge exponentially to the steady state velocity

$$\overline{v} = -\mathcal{A}^{-1}b = \begin{bmatrix} \overline{v}_t & \overline{v}_n & \overline{v}_\theta \end{bmatrix}^T \tag{77}$$

which is given analytically by

$$\overline{v}_t = k_{\alpha\omega}k_\delta\frac{Nc_nc_p}{2\left(N^2c_tc_n - (4N^2-8N+4)c_p^2\phi_o^2\right)} \tag{78a}$$

$$\overline{v}_n = k_{\alpha\omega}k_\delta\frac{\phi_o\left(N-1\right)c_p^2}{N^2c_tc_n - (4N^2-8N+4)c_p^2\phi_o^2} \tag{78b}$$

$$\overline{v}_\theta = k_{\alpha\omega}k_\delta\frac{\phi_oNc_nc_p\lambda_2}{2\lambda_1\left(N^2c_tc_n - (4N^2-8N+4)c_p^2\phi_o^2\right)} \tag{78c}$$

We can see that the resulting steady state velocity of the snake robot is proportional to the controller parameters $k_{\alpha\omega} = \alpha^2\omega$ and k_δ, and that the velocity also depends on nonlinear terms involving the joint coordinate offset ϕ_o.

Since the averaged model of the velocity dynamics given by (73) is *globally exponentially stable* (assuming that (76) is satisfied), it follows from Theorem 19 that, for sufficiently small ε (i.e. for sufficiently large ω), the average velocity given by (73) will approximate the exact velocity (60) for all time, and that the error of this approximation is of order ε, i.e. bounded in accordance with (58). In this paper, we will not investigate the lower limit of ω corresponding to some maximum error bound.

However, the simulation results presented in Section X show that the exact and the average velocity agree well when ω is set to values that are commonly used for snake robot locomotion.

We now summarize the above conclusions.

Proposition 21: Consider a planar snake robot described by (47). Suppose the joint coordinates ϕ are controlled in exact accordance with (6) and (7), and that the joint coordinate offset ϕ_o satisfies (76). Then there exist $k > 0$ and $\omega^* > 0$ such that for all $\omega > \omega^*$,

$$\|\boldsymbol{v}(t) - \boldsymbol{v}_{av}(t)\| \leq \tfrac{k}{\omega} \quad \text{for all } t \in [0, \infty) \tag{79}$$

where $\boldsymbol{v}(t)$ denotes the exact velocity of the snake robot given by (60) and $\boldsymbol{v}_{av}(t)$ denotes the average velocity given by (73). Furthermore, the average velocity $\boldsymbol{v}_{av}(t)$ of the snake robot will converge exponentially fast to the steady state velocity $\overline{\boldsymbol{v}}$ given by (77).

E. Fundamental relationships between the gait parameters and the forward velocity

Proposition 21 is a powerful result. First of all, it proves mathematically that lateral undulation enables a wheel-less snake robot with anisotropic ground friction properties to achieve forward propulsion (under the assumption that the body shape motion is modelled as translational link displacements). Second, the result gives an analytical expression for the steady state velocity as a function of the controller parameters α, ω, δ, and ϕ_o, i.e. the amplitude, frequency, phase shift and offset of the joint motion during lateral undulation. This information is relevant for motion planning purposes. We can for example immediately see from (77) that the steady state velocity of the snake robot when it conducts lateral undulation with zero joint offset ($\phi_o = 0$) is given by $\overline{v}_t = \frac{c_p}{2Nc_t} k_{\alpha\omega} k_\delta$, $\overline{v}_n = 0$, and $\overline{v}_\theta = 0$. A final powerful feature of Proposition 21 is that it applies to snake robots with an arbitrary number of links N.

In the following, we will use Proposition 21 to deduce some fundamental relationships between the forward velocity and the controller parameters of the snake robot. The forward velocity is seen from (78a) to be proportional to the controller parameter $k_{\alpha\omega} = \alpha^2 \omega$, i.e. the forward velocity is proportional to the square of the amplitude of the joint motion, α^2, and also proportional to the angular frequency, ω, of the joint motion. This information is useful from a motion planning perspective since it tells us that an increase/decrease of the forward velocity by a certain factor can be achieved by increasing/decreasing ω by the same factor or by increasing/decreasing α by the square root of this factor.

It is also seen from (78a) that the forward velocity of the snake robot is proportional to the function k_δ defined in (69). Since k_δ is a function of the phase shift δ between the joints, this means that the phase shift δ that will maximize the forward velocity can be determined as the δ that maximizes k_δ.
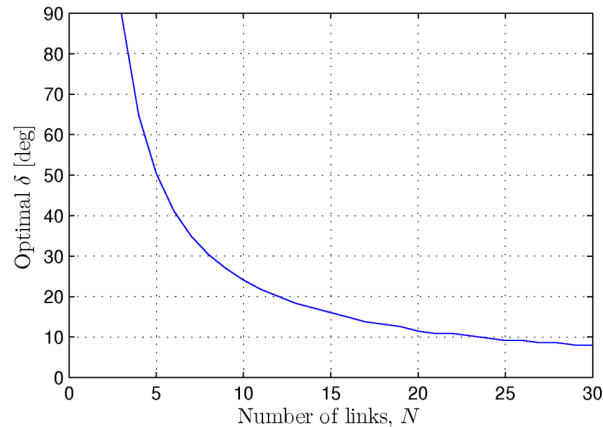
Fig. 13. The optimal phase shift δ that maximizes the forward velocity of a planar snake robot as a function of the number of links N.

This is particularly interesting since we are now able to use the analytical expression of k_δ to determine the optimal phase shift δ that maximizes the forward velocity of a planar snake robot with an arbitrary number of links N. Fig. 13 presents a plot of the maximum value of k_δ as a function of the number of links N. For each N, the maximum value of k_δ was found using the mathematical computer software *Matlab*. The optimal phase shift is e.g. $\delta = 90°$ for $N = 3$ links, $\delta = 50.4°$ for $N = 5$ links, $\delta = 24.1°$ for $N = 10$ links, and $\delta = 11.5°$ for $N = 20$ links.

The above results can be summarized as follows:

Proposition 22: Consider a planar snake robot with N links modelled by (47) and controlled in exact accordance with (6) and (7). The average forward velocity of the snake robot given by (73) will converge exponentially to a value which is proportional to:

- the squared amplitude of the sinusoidal joint motion, α^2.

- the angular frequency of the sinusoidal joint motion, ω.

- the function of the constant phase shift, δ, between the joints given by

$$k_\delta = \sum_{i=1}^{N-1}\sum_{j=1}^{N-1} a_{ij} \sin\left((j-i)\,\delta\right) \tag{80}$$

where a_{ij} denotes element ij of the matrix $A\overline{D}$. Moreover, for a given α and ω, the phase shift, δ, that maximizes the average forward velocity is given by the δ that maximizes k_δ.

IX. Simulation study: Comparison between the complex and the simplified model

This section presents simulation results in order to compare the complex snake robot model given by (5) with the simplified model given by (47).

Remark 23: As noted in Remark 11 in Section V-D2, we have not specified how to set the rotation parameters λ_1 and λ_2 as a function of the remaining parameters of the snake robot. However, knowing this mapping is not critical to the intended use of the simplified model for controller design purposes as long as we know that the *qualitative* and the approximate *quantitative* behaviour of the complex model is *contained* within the simplified model for some choice of numerical values of the parameters λ_1 and λ_2. The purpose of this section is to illustrate this qualitative and quantitative similarity between the two models.

A. Simulation parameters

Both models were implemented and simulated in *Matlab R2011a* on a laptop running *Windows XP*. The dynamics was calculated using the *ode45* solver in Matlab with a relative and absolute error tolerance of 10^{-6}. We considered a snake robot with $N = 10$ links of length $l = 0.14$ m and mass $m = 1$ kg. The links of the snake robot in the complex model had moment of inertia $J = 0.0016$ kgm^2. The ground friction coefficients were $c_t = 1$ and $c_n = 3$, and the rotation parameters of the simplified model were $\lambda_1 = 0.5$ and $\lambda_2 = 20$. Both models were simulated with the joint controller given by (9) with controller gains $k_p = 20$ and $k_d = 5$. In order to compare the two models, we controlled the snake robot in both models according to the gait pattern lateral undulation defined in (6). The angular frequency and phase shift of the gait pattern were $\omega = 120°$/s and $\delta = 40°$, respectively, while the amplitude α and the joint offset ϕ_o are presented with each simulation result below.

B. Relationship between the joint coordinates in the complex and simplified model

In order to illustrate the range of link angles where the simplified model agrees with the complex model, we carried out simulations of lateral undulation where the amplitude of the link angles was $\theta_i = 10°$, $15°$, $20°$, and $30°$, respectively, for $i \in \{1, \cdots, N\}$. For the kinematic parameters and gait parameters listed in Section IX-A, these link angle amplitudes are achieved in the complex model by choosing the amplitude α in (6) as $\alpha = 7.1°$, $10.5°$, $13.9°$, and $21°$, respectively. Furthermore, these link angle amplitudes will cause the amplitudes of the normal direction distance between the links (i.e. the amplitude of the joint coordinates in the simplified model) to be $y_{i+1} - y_i = 2.3$ cm, 3.4 cm, 4.5 cm, and 6.6 cm, respectively. These relationships are shown in Fig. 14 and were found through trial and

error by simulating the complex model of the snake robot with the parameters listed in Section IX-A. In particular, the figure shows a simulation of the complex model where the snake robot first conducts lateral undulation with $\alpha = 7.1°$ for 30 s, then with $\alpha = 10.5°$ for 30 s, then with $\alpha = 13.9°$ for 30 s, and finally with $\alpha = 21°$ for 30 s. Fig. 14(a) shows the maximum value of all the N link angles at each timestep, while Fig. 14(b) shows the maximum value of the normal direction distance between the links at each timestep. The link angle amplitude and the normal direction link distance corresponding to each value of α were estimated as the average of the plotted values inside each 30 s time interval.

In summary, Fig. 14 shows that lateral undulation with the kinematic parameters and gait parameters listed in Section IX-A, where the amplitude of the link angles are $\theta_i = 10°$, $15°$, $20°$, and $30°$, respectively, is achieved in the complex model by choosing the amplitude α in (6) as $\alpha = 7.1°$, $10.5°$, $13.9°$, and $21°$, respectively, and is achieved in the simplified model by choosing the amplitude α in (6) as $\alpha = 2.3$ cm, 3.4 cm, 4.5 cm, and 6.6 cm, respectively.

C. Comparison of straight motion

We begin by comparing the complex and the simplified model during lateral undulation along a straight line. The amplitude α in (6) was set in intervals of 45 s according to the values derived for both models in the previous subsection, i.e. $\alpha = 7.1°$, $10.5°$, $13.9°$, and $21°$, respectively, for the complex model and $\alpha = 2.3$ cm, 3.4 cm, 4.5 cm, and 6.6 cm, respectively, for the simplified model. The joint offset ϕ_o in (6) was set to zero in both models. The snake robot in the complex model started moving from $(p_x = 0, p_y = -0.5)$, while the snake robot in the simplified model started moving from $(p_x = 0, p_y = 0.5)$. Both snake robots were initially headed along the global x axis with zero joint coordinates.

The simulaton result is shown in Fig. 15, where the plots on the right side are normalized with respect to body length in order to remove the effect of the body length extension issue explained in Section V-F2. In particular, while the body length of the snake robot with revolute joints in the complex model is constant and given by (49), the body length of the prismatic snake robot in the simplified model will slightly increase according to (50) for increasing joint coordinates. In order to remove the effect of this extension issue when comparing the two models, we normalize the simulation result by dividing the simulated state values by the body length at each time step, given by (49) and (50) for the complex and the simplified model, respectively. Each plot to the right in Fig. 15 is the normalized plot of the corresponding plot to the left.

The motion of the CM of the two robots is plotted in Figures 15(a) and (b), where the configuration of the snake robots is visualized in the middle of each 45 s time interval. Furthermore, Figures 15(c)-(f)
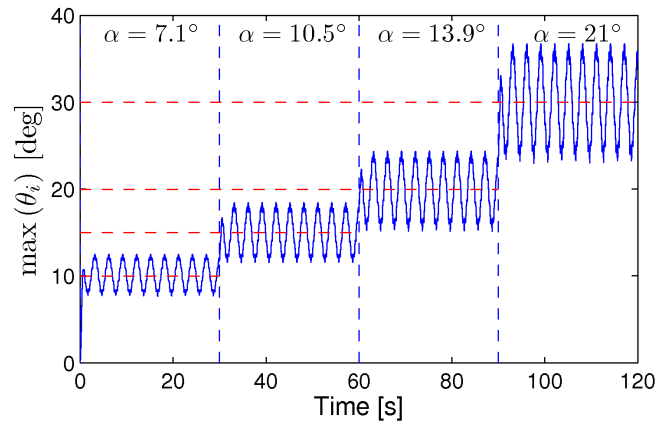
(a) The link angle amplitudes $\theta_i = 10°$, $15°$, $20°$, and $30°$ are achieved by choosing the joint angle amplitudes as $\alpha = 7.1°$, $10.5°$, $13.9°$, and $21°$, respectively.
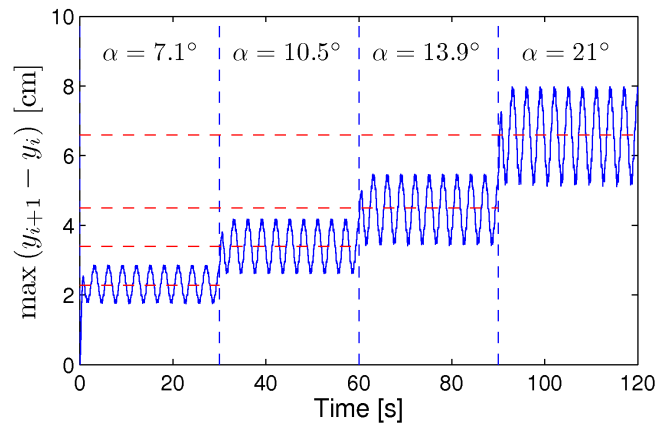
(b) The estimated amplitudes of the normal direction distance between the links at each of the four joint angle amplitudes are, respectively, $y_{i+1} - y_i = 2.3$ cm, 3.4 cm, 4.5 cm, and 6.6 cm.

Fig. 14. A simulation of the complex model where the snake robot conducts lateral undulation at four different joint angle amplitudes. The plots show the corresponding amplitudes of the link angles (top) and the amplitudes of the normal direction distances between the links (bottom).

show the CM velocity of the snake robots in the global x and y direction, respectively. The body length of the snake robot at each time step is plotted in Fig. 16.

The simulation results indicate that the forward motion dynamics of the simplified model agrees well with the complex model as long as the link angles are limited. In particular, there is a good agreement between the two models in the two first time intervals, where the link angle amplitude is $10°$ and $15°$, respectively. In the third time interval, where the link angle amplitude is increased to $20°$, the forward velocity in the two models begin to deviate. This deviation is increased in the fourth and last time interval, where the link angle amplitude is increased to $30°$. These observations also apply to the normalized plots on the right side.

These simulation results agree very well with the predictions that were made in conjunction with the derivation of the simplified model. In particular, Fig. 10 suggests that the ground friction forces in the simplified model rely on approximations which are valid for link angles limited by approximately $|\theta_i| < 20°$. The simulation result in Fig. 15 supports this conjecture. The agreement between the two models is slightly improved in the normalized plots, but not to a very large extent, which supports our conjecture in Section V-F2 that the effect of the extension issue of the prismatic snake robot is small as long as the joint coordinates are limited.

Notice that the velocity plots from the complex model contain high-frequency components which are not visible in the plots from the simplified model. This indicates that the complex model contains nonlinear components which are not included in the simplified model. However, the similar behaviour of the two models at limited link angles indicates that the simplified model captures the parts of the complex model that determine the overall motion of the snake robot. This suggests that we may use the simplified model to develop general analysis and control design results that will also apply to the complex model.

D. Comparison of turning motion

In the next simulation, we compare the complex and the simplified model during lateral undulation involving turning motion. In order to induce turning motion, the joint offset ϕ_o in (6) was set to $\phi_o = \frac{1}{3}\alpha$ in the time interval $t \in [40, 70]$ and $\phi_o = -\frac{1}{3}\alpha$ in the time interval $t \in [130, 160]$. The offset was zero outside these two time intervals. To compare the models at different link angle amplitudes, the simulation was carried out three times with link angle amplitude $\theta_i = 10°$, $20°$, and $30°$, respectively, for $i \in \{1, \cdots, N\}$. The corresponding amplitude α in (6) was set according to the values derived in Section IX-B, i.e. $\alpha = 7.1°$, $13.9°$, and $21°$, respectively, for the complex model and $\alpha = 2.3$ cm, 4.5 cm, and 6.6 cm, respectively, for the simplified model. All intial state values of the snake robot were
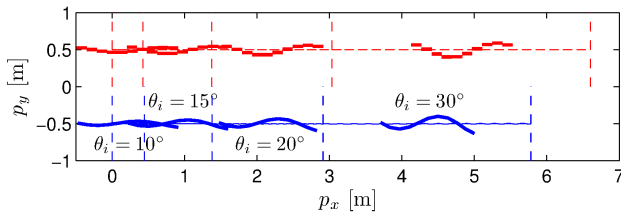
(a) The CM position from the complex (bottom) and simplified (top) model.
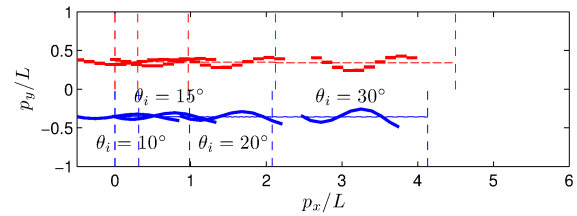
(b) The normalized CM position from the complex (bottom) and simplified (top) model.
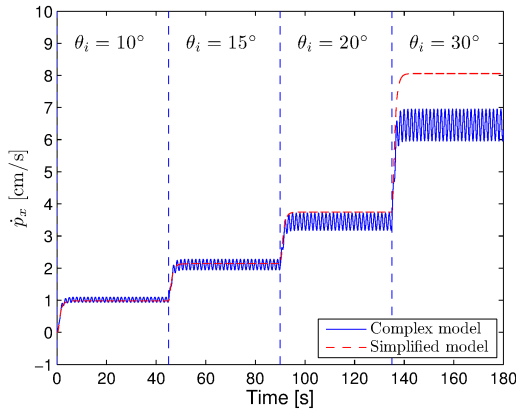
(c) The CM velocity in the global x direction, $\dot{p}_x$.
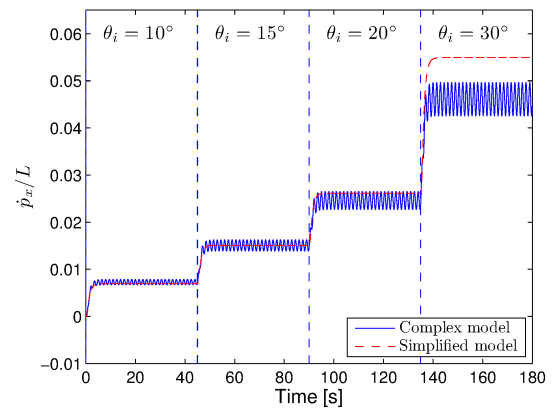
(d) The normalized CM velocity in the global x direction, $\dot{p}_x/L$.
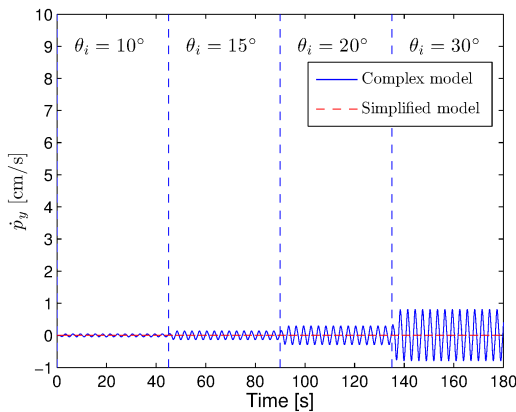
(e) The CM velocity in the global y direction, $\dot{p}_y$.
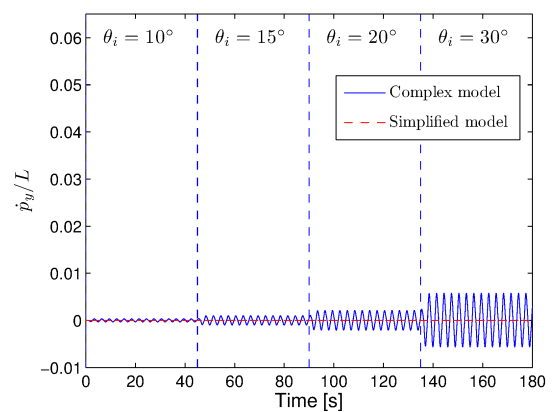
(f) The normalized CM velocity in the global y direction, $\dot{p}_y/L$.

Fig. 15. Simulation results which compare the complex and the simplified model during lateral undulation along a straight line at four different link angle amplitudes. The normalized quantities in the plots to the right are calculated by dividing the state values by the body length of the snake robot at each time step.
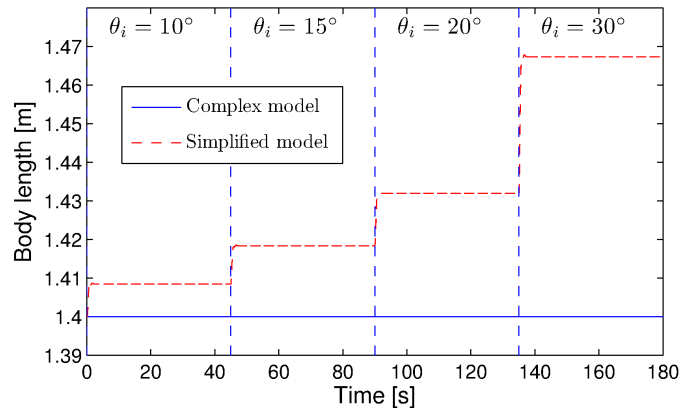
Fig. 16. The body length of the snake robot during lateral undulation along a straight line at four different link angle amplitudes.

zero.

The simulation results from the three trials are shown in Fig. 17, Fig. 18, and Fig. 19, respectively, where we also present plots which are normalized with respect to body length in order to remove the effect of the body length extension issue explained in Section V-F2. As explained in the previous subsection, the normalized plots are produced by dividing the simulated state values by the body length at each time step, given by (49) and (50) for the complex and the simplified model, respectively.

In all three figures, the motion of the CM of the two robots is plotted in subfigures (a) and (b), where the snake robot from the complex model is visualized at $t = 5$ s and the snake robot from the simplified model is visualized at $t = 195$ s. Furthermore, subfigures (c)-(f) show the CM velocity of the snake robots, while subfigure (g) shows the orientation of the snake robots, which was given by θ in the simplified model, and which was estimated as the average of the link angles in the complex model, i.e. as $\bar{\theta} = \frac{1}{N} \sum_{i=1}^{N} \theta_i$. Finally, subfigure (h) shows the body length of the snake robot at each time step, which is constant for the snake robot in the complex model, but which varies according to (50) for the simplified model.

In all three simulation trials, the *qualitative* behaviour of the snake robot from the simplified model is similar to the behaviour from the complex model. With the chosen numerical values of the rotation parameters λ_1 and λ_2 in the simplified model, we also achieved a good *quantitative* similarity between the two models. We can see that the quantitative similarity is best in the first trial, where the link angle amplitude is $10°$, and that there is some deviation between the two models in the second trial, where the link angle amplitude is $20°$. The deviation is even larger in the third trial, where the link angle

amplitude is $30°$. Again, these results agree with the predictions that were made in conjunction with the derivation of the simplified model, namely that the *quantitative* agreement between the complex and the simplified model is best for link angles limited by approximately $|\theta_i| < 20°$. Note that we also predicted that the two models will be *qualitatively* similar also for link angles above this approximate bound. The simulation result in Fig. 19 supports this conjecture since the *qualitative* behaviours of the two snake robots are similar even though there is a *quantitative* discrepancy between the plots. Note that the quantitative agreement between the two models is slightly improved in the normalized plots, but not to a very large extent, which supports our conjecture in Section V-F2 that the effect of the extension issue of the prismatic snake robot is small as long as the joint coordinates are limited.

X. SIMULATION STUDY: INVESTIGATION OF THE AVERAGED VELOCITY DYNAMICS

This section presents simulation results in order to investigate the validity of Proposition 21, i.e. to validate the agreement between the original simplified model (47) and the averaged model (73).

A. Simulation parameters

The original model of the snake robot was given by (47) under the assumption that ϕ was controlled in exact accordance with (6). The averaged model of the snake robot was given by (73). The ground friction coefficients were $c_t = 0.5$ and $c_n = 3$, and the rotation parameters were $\lambda_1 = 0.5$ and $\lambda_2 = 20$. The remaining simulation parameters were identical to the parameters presented in Section IX-A except for the values of the gait parameters α, ω, δ, and ϕ_o, which are presented with each simulation result below.

B. Simulation results

The motion of the snake robot during lateral undulation was first simulated with the controller parameters $\alpha = 0.05$ m, $\omega = 70°/s$, $\delta = 40°$, and $\phi_o = l/8$ m. The joint coordinates were, in other words, offseted by $1/8$ of the link length l. In accordance with Proposition 21, the average velocity of the snake robot should then converge exponentially fast to the steady state velocity $\overline{v}_t = 7.12$ cm/s, $\overline{v}_n = 0.67$ cm/s, and $\overline{v}_\theta = 2.86°/s$. This prediction agrees very well with the simulation result shown in Fig. 20. The top left plot shows the global CM position of the snake robot and also the body shape at $t = 5$ s and $t = 40$ s, while the other three plots show the velocities from the original and the averaged model. The close overlap between the velocity plots from the two models suggests that $\omega = 70°/s$ is well above the (unknown) value of ω^* described in Proposition 21.
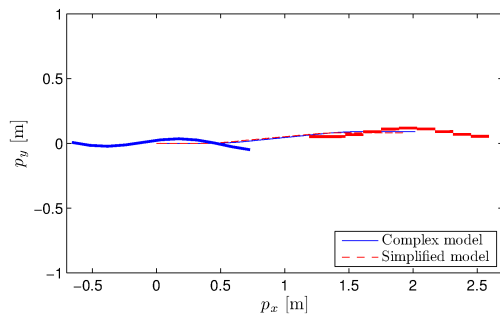
(a) The CM position.
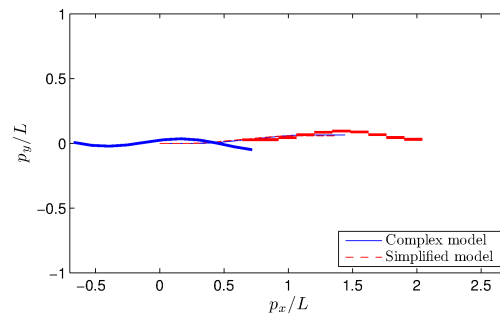
(b) The normalized CM position.
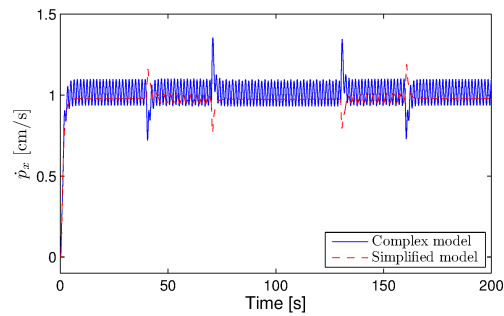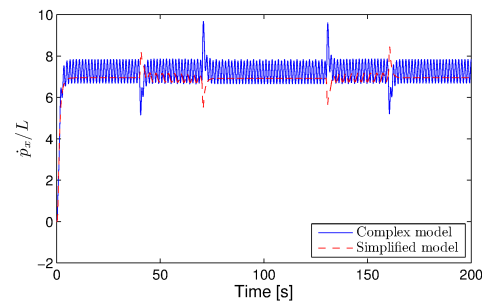
(c) The CM velocity, $\dot{p}_x$.

(d) The normalized CM velocity, $\dot{p}_x/L$.
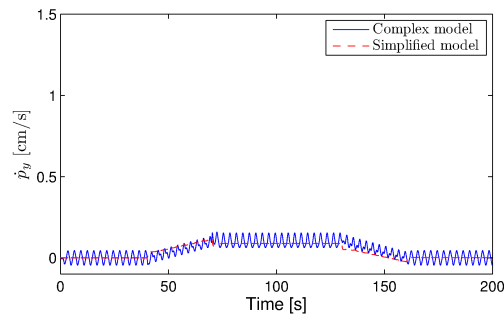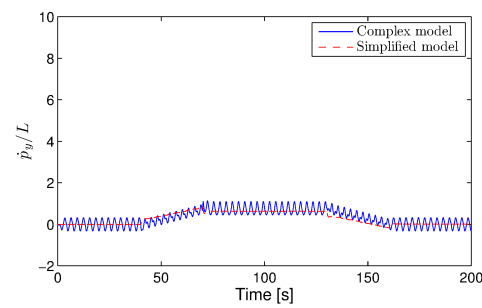
(e) The CM velocity, $\dot{p}_y$.

(f) The normalized CM velocity, $\dot{p}_y/L$.
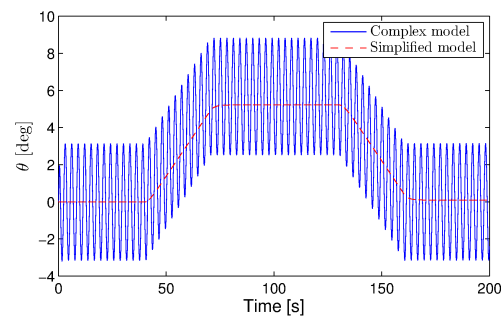
(g) The orientation of the snake robot.
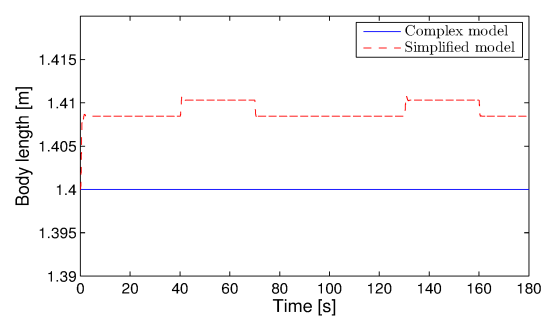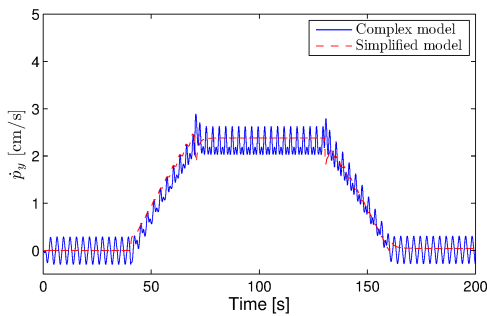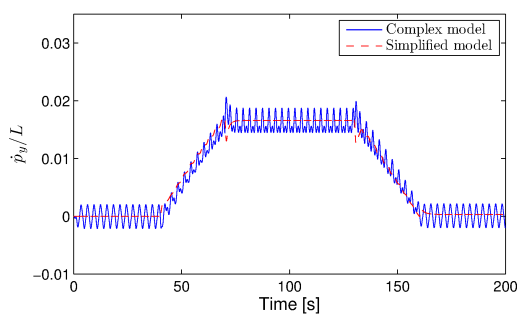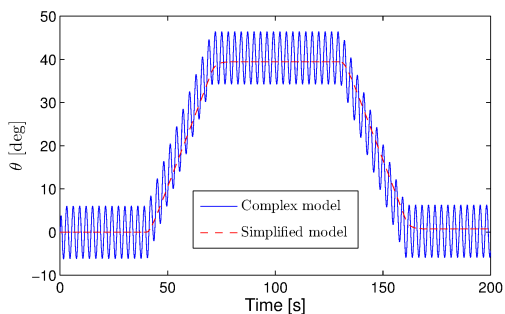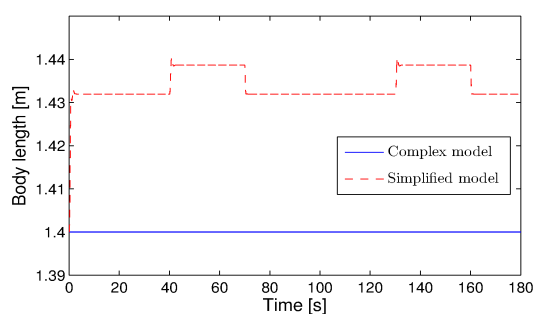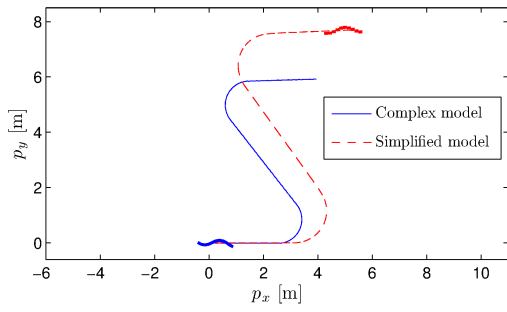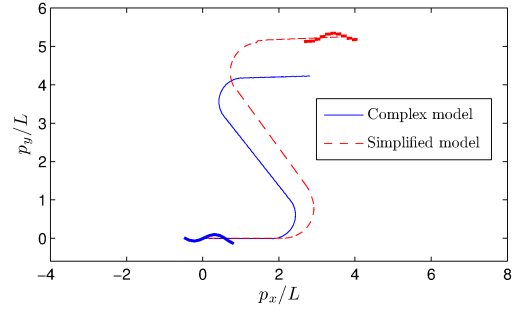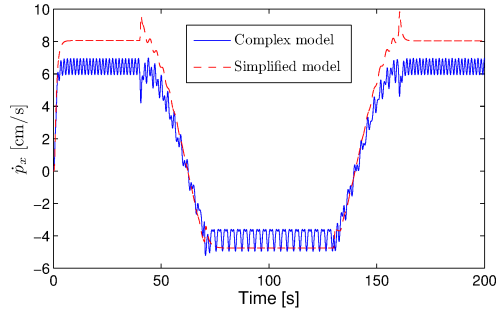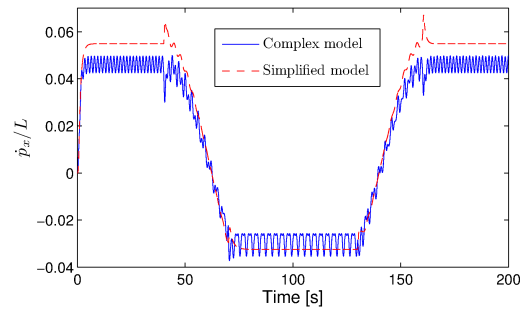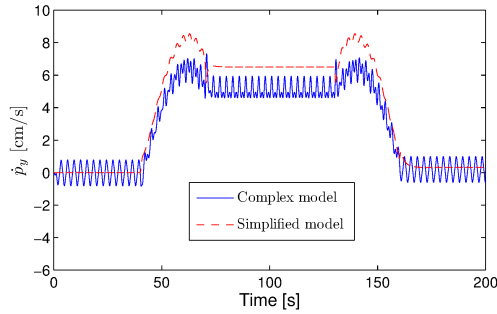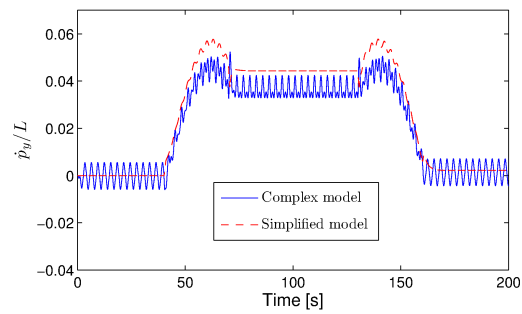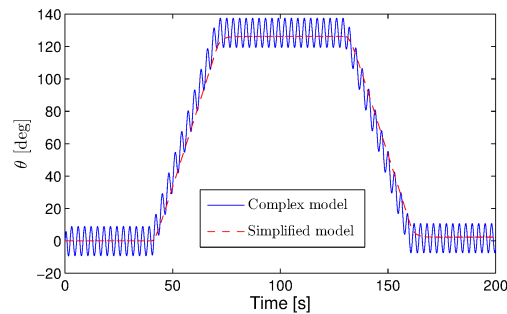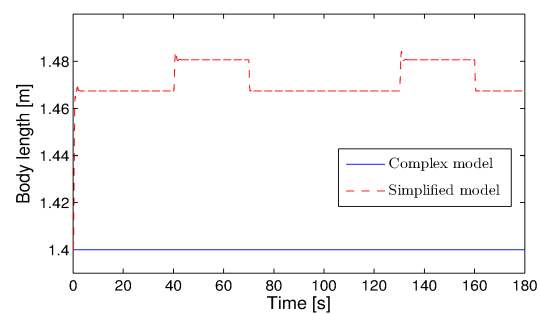
(h) The body length of the snake robot.

Fig. 17. Simulation results which compare the complex and the simplified model during turning motion. The amplitude of the link angles is $\theta_i = 10°$. The normalized quantities in the plots to the right are calculated by dividing the state values by the body length of the snake robot at each time step.
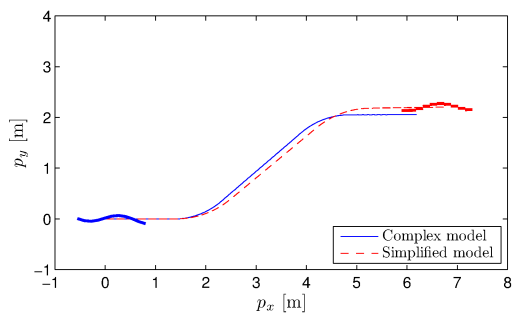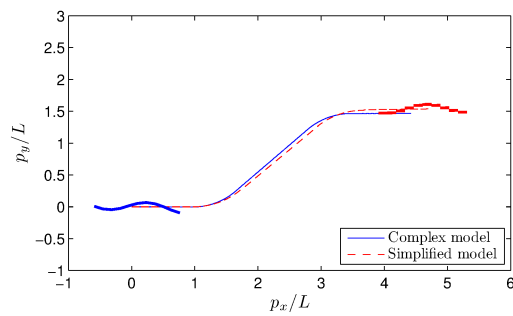
(a) The CM position.

(b) The normalized CM position.
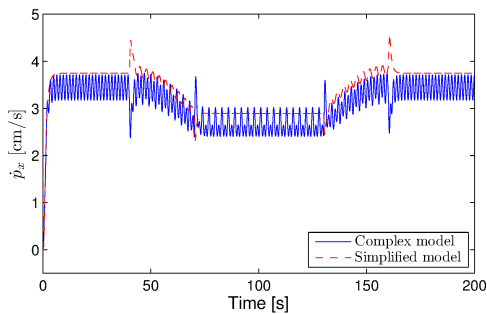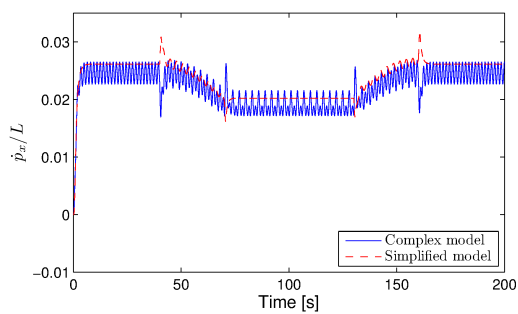
(c) The CM velocity, $\dot{p}_x$.

(d) The normalized CM velocity, $\dot{p}_x/L$.

(e) The CM velocity, $\dot{p}_y$.

(f) The normalized CM velocity, $\dot{p}_y/L$.

(g) The orientation of the snake robot.

(h) The body length of the snake robot.

Fig. 18.   Simulation results which compare the complex and the simplified model during turning motion. The amplitude of the link angles is $\theta_i = 20°$. The normalized quantities in the plots to the right are calculated by dividing the state values by the body length of the snake robot at each time step.

(a) The CM position.

(b) The normalized CM position.

(c) The CM velocity, $\dot{p}_x$.

(d) The normalized CM velocity, $\dot{p}_x/L$.

(e) The CM velocity, $\dot{p}_y$.

(f) The normalized CM velocity, $\dot{p}_y/L$.

(g) The orientation of the snake robot.

(h) The body length of the snake robot.

Fig. 19. Simulation results which compare the complex and the simplified model during turning motion. The amplitude of the link angles is $\theta_i = 30°$. The normalized quantities in the plots to the right are calculated by dividing the state values by the body length of the snake robot at each time step.

In the second simulation, the controller parameters were set to $\alpha = 0.05$ m, $\omega = 30°/$s, $\delta = 40°$, and $\phi_o = -l/4$ m. The joint coordinates were, in other words, offseted by $1/4$ of the link length l. In addition, we reduced the frequency of the sinusoidal motion from $\omega = 70°/$s to $\omega = 30°/$s to see how this affected the estimate of the average velocity. From Proposition 21, the average velocity should converge to $\overline{v}_t = 3.66$ cm/s, $\overline{v}_n = -0.69$ cm/s, and $\overline{v}_\theta = -2.94°/$s. This agrees very well with the simulation result shown in Fig. 21. The figure shows that there is still a good agreement between the velocities from the original and the averaged model even though we reduced ω considerably.

XI. Simulation study: Investigation of the relationships between gait parameters and forward velocity

This section presents simulation results in order to investigate the validity of Proposition 22, i.e. the validity of the relationships between the gait pattern parameters of lateral undulation and the resulting forward velocity of the snake robot. In addition to validating the relationships in Proposition 22 with simulation results from the simplified model (47), this section also shows that the relationships apply to the velocity from the complex model given by (5).

Remark 24: The joint coordinates of the simplified model (normal direction link distances) are different from the joint coordinates of the complex model (joint angles). However, it still makes sense to investigate the validity of Proposition 22 for a snake robot with revolute joints since, as implied by Property 6, the rotational link motion is what produces the linear displacements captured by the simplified model. Note also that for limited link angles, there is approximately a linear relationship between the amplitude of the angular joint motion and the corresponding amplitude of the transversal link displacments. The relationship stated in Proposition 22 between the forward velocity and the squared amplitude of the sinusoidal joint motion, α^2, can therefore be expected to hold also when α denotes the amplitude of the angular joint motion of a snake robot with revolute joints.

A. Simulation parameters

The complex model (5) and the simplified model (47) were implemented and simulated in *Matlab R2008b* on a laptop running *Windows XP*. The dynamics was calculated using the *ode45* solver in Matlab with a relative and absolute error tolerance of 10^{-3} and 10^{-6} in the complex and the simplified model, respectively.

We considered snake robots with $N = 3$, $N = 5$, $N = 10$, and $N = 20$ links of length $l = 0.14$ m, mass $m = 1$ kg, and moment of inertia $J = 0.0016$ kgm^2. The ground friction coefficients were $c_t = 1$
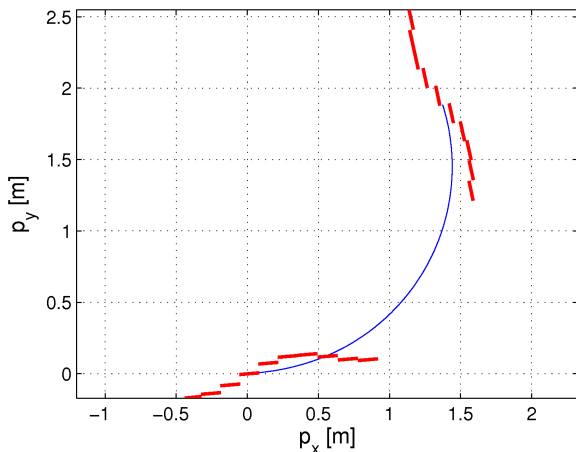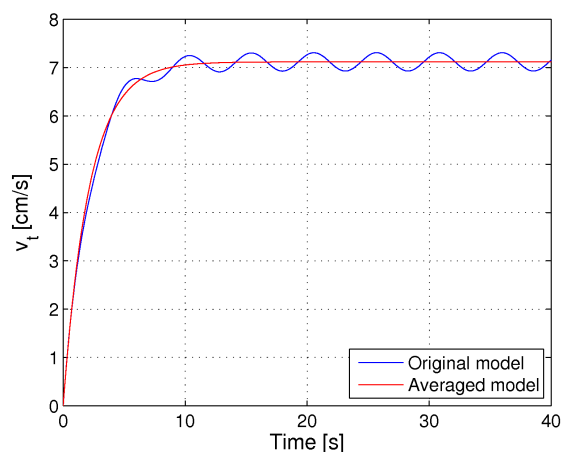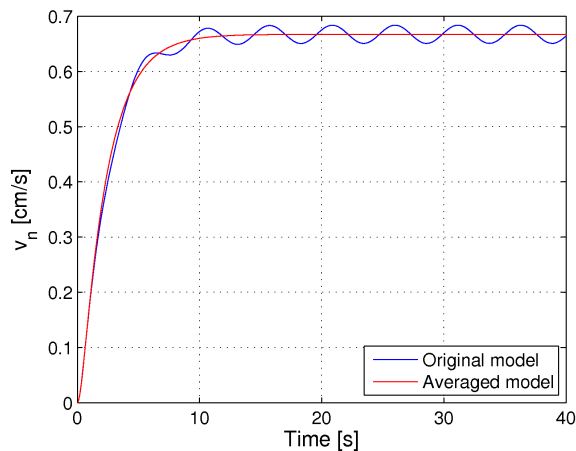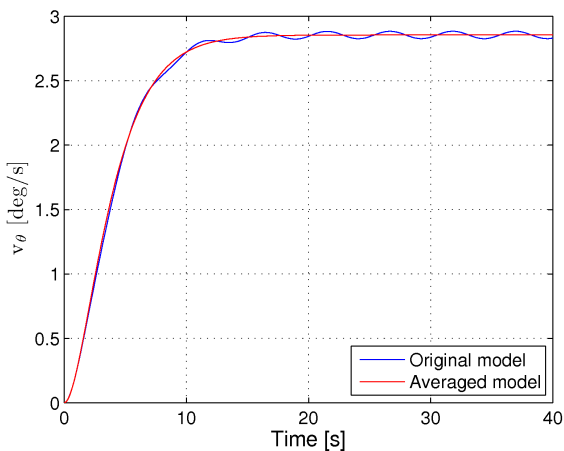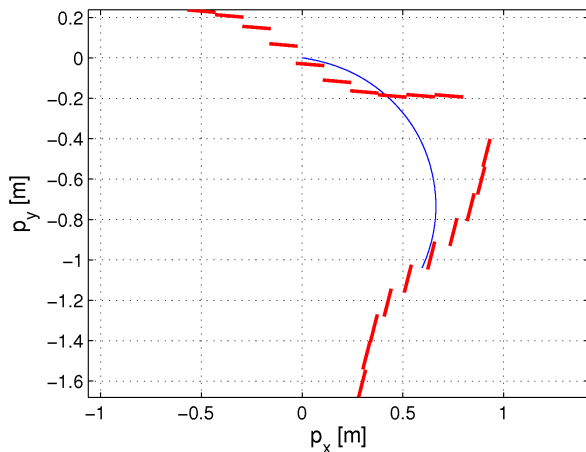
(a) The CM position of the snake robot.

(b) The forward velocity v_t.

(c) The sideways velocity v_n.

(d) The rotation velocity v_θ.

Fig. 20. Comparison between the original simplified model and the averaged model for counterclockwise turning motion with controller parameters $\alpha = 0.05$ m, $\omega = 70°/s$, $\delta = 40°$, and $\phi_o = l/8$ m.

and $c_n = 3$, and the rotation parameters of the simplified model were $\lambda_1 = 0.5$ and $\lambda_2 = 20$. Both models were simulated with the joint controller given by (9) with controller gains $k_p = 20$ and $k_d = 5$. The joint reference coordinates were calculated according to the motion pattern lateral undulation defined in (6) with zero joint angle offset ($\phi_o = 0$). The values of the gait pattern parameters α, ω, and δ are presented with each simulation result. All intial state values of both models were zero.

The simulation results below present the forward velocity of the snake robot, denoted by $\bar{v}$, for different

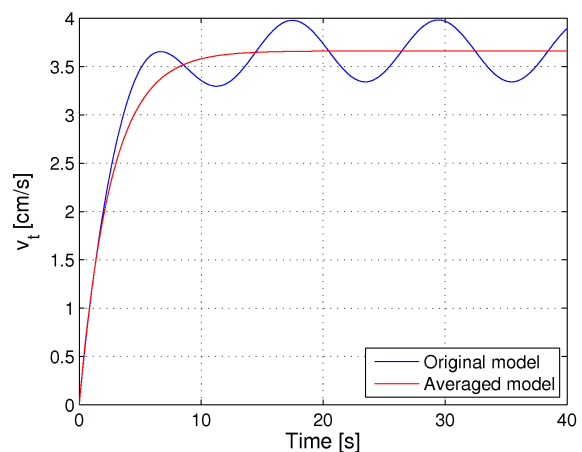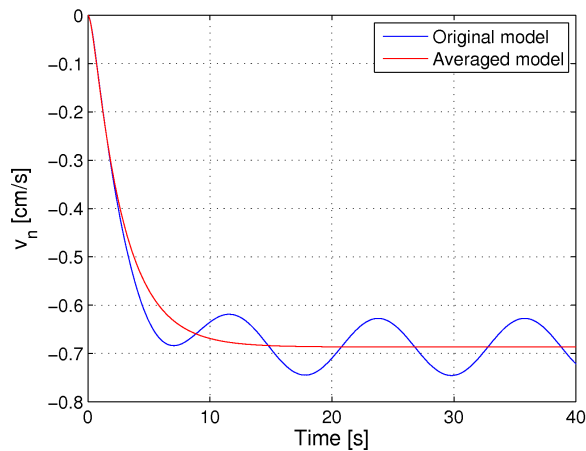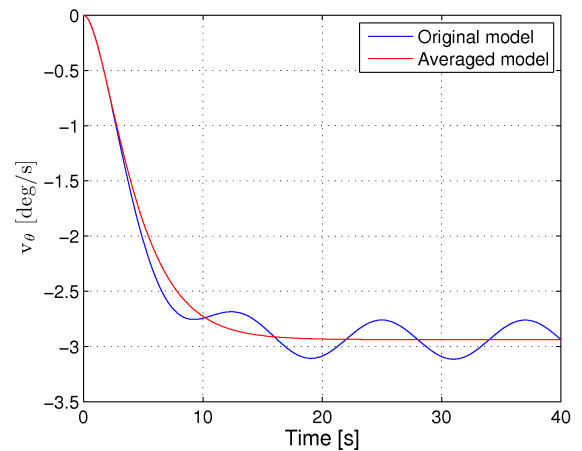(a) The CM position of the snake robot.

(b) The forward velocity v_t.

(c) The sideways velocity v_n.

(d) The rotation velocity v_θ.

Fig. 21. Comparison between the original simplified model and the averaged model for clockwise turning motion with controller parameters $\alpha = 0.05$ m, $\omega = 30°/$s, $\delta = 40°$, and $\phi_o = -l/4$ m.

sets of gait pattern parameters. The velocity was calculated at the end of each simulation trial as the linear distance travelled by the CM of the snake robot divided by the simulation time, which was chosen to be $t_{\text{sim}} = 10$ s. In other words, the velocity was calculated as

$$\overline{v} = \frac{\sqrt{\left(p_x\left(10\right) - p_x\left(0\right)\right)^2 + \left(p_y\left(10\right) - p_y\left(0\right)\right)^2}}{10} \tag{81}$$

Note that the velocity in each plot is presented in terms of body length units in order to generalise the

results. In particular, we define the body length of the snake robot in both the simplified and the complex model as

$$L = Nl \tag{82}$$

Consequently, the velocity in body length units is given as $\overline{v}/L$.

Remark 25: The essence of the simulation results presented in this section is contained in the particular shape of each graph, which means that a quantitative comparison between the graphs from the complex and the simplified model is not relevant. The values of the amplitude α of the joint motion in the complex model were therefore set independently from the values of α in the simplified model.

B. Relationship between the forward velocity and α

Proposition 22 states that the average forward velocity of a planar snake robot is proportional to the squared amplitude of the sinusoidal joint motion, α^2. We investigated the validity of this result by simulating the snake robot with different values of α and calculating the resulting average forward velocity. We considered snake robots with $N = 3$, 5, 10, and 20 links, respectively, with $\delta = 90°$, $50.4°$, $24.1°$, and $11.5°$, respectively, and with $\omega = 70°$/s. The simulation results from the simplified model are shown in Fig. 22(a), while the simulation results from the complex model are shown in Fig. 22(b). In the plots from the complex model, the range of α values is shorter for large N compared to for small N since a large angle amplitude would cause a collision between the head and the tail of the snake when N is large. Note also that the joint amplitudes α in the plots from the simplified model are given in terms of body length units. The plots show a quadratic increase in the forward speed as the amplitude α increases. This is in accordance with Proposition 22.

Note that the amplitude of the joint motion cannot be increased indefinitely in the complex model. For sufficiently large α, the relative link velocity components that are *tangential* to the forward direction will no longer be negligible, which is assumed in the simplified model of the snake robot. It is therefore reasonable to expect that the increase in the forward velocity from the complex model will decay for large α. This decay is slightly seen in the plots in Fig. 22(b), which shows that the increase of the velocity has a more linear than quadratic characteristic when α becomes large.

C. Relationship between the forward velocity and ω

Proposition 22 states that the average forward velocity of a planar snake robot is proportional to the angular frequency, ω, of the joint motion. This result was investigated by simulating the snake robot
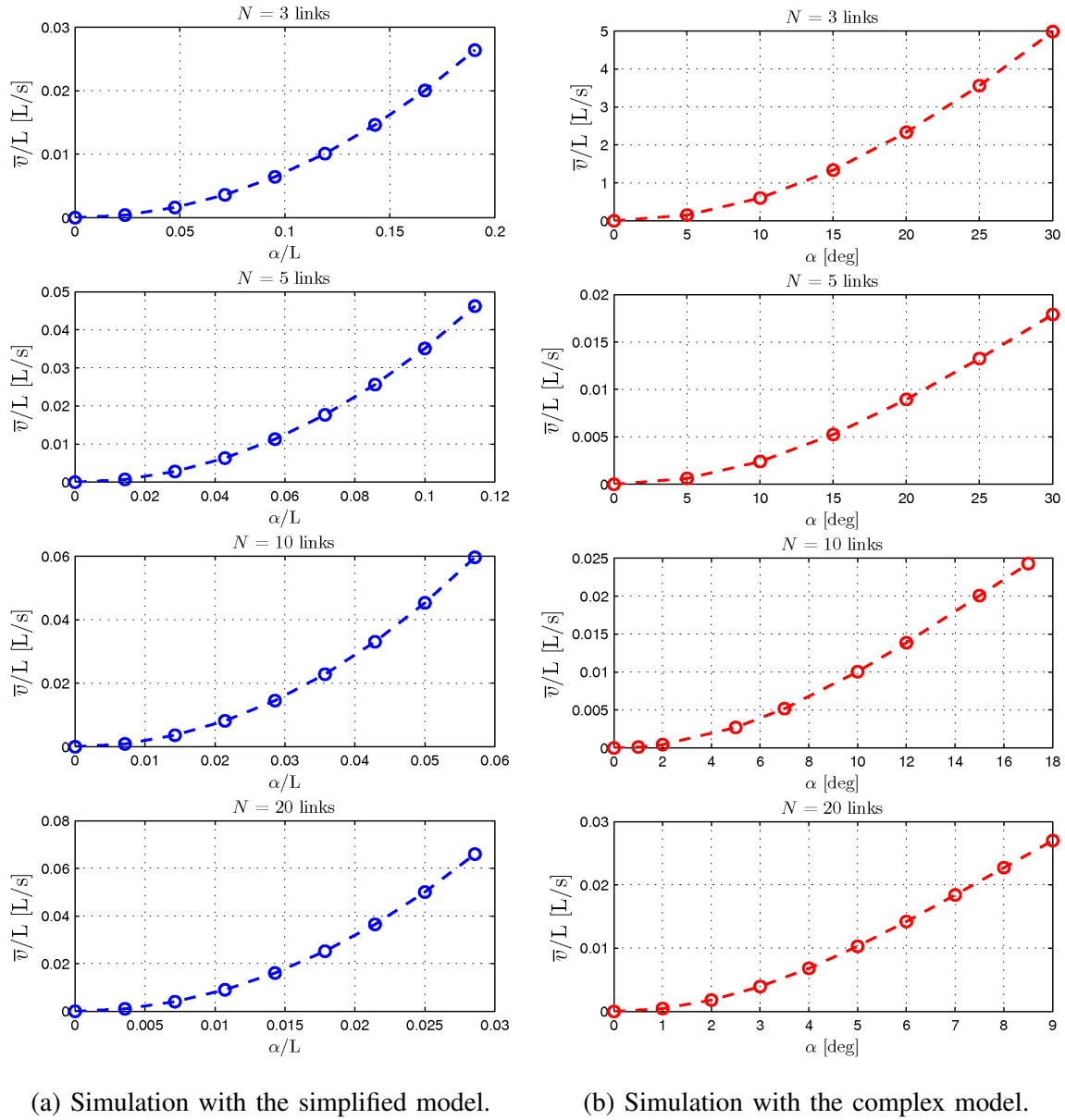
(a) Simulation with the simplified model.

(b) Simulation with the complex model.

Fig. 22. The forward velocity of the snake robot for different values of α. The number of links N are shown at the top of each plot.
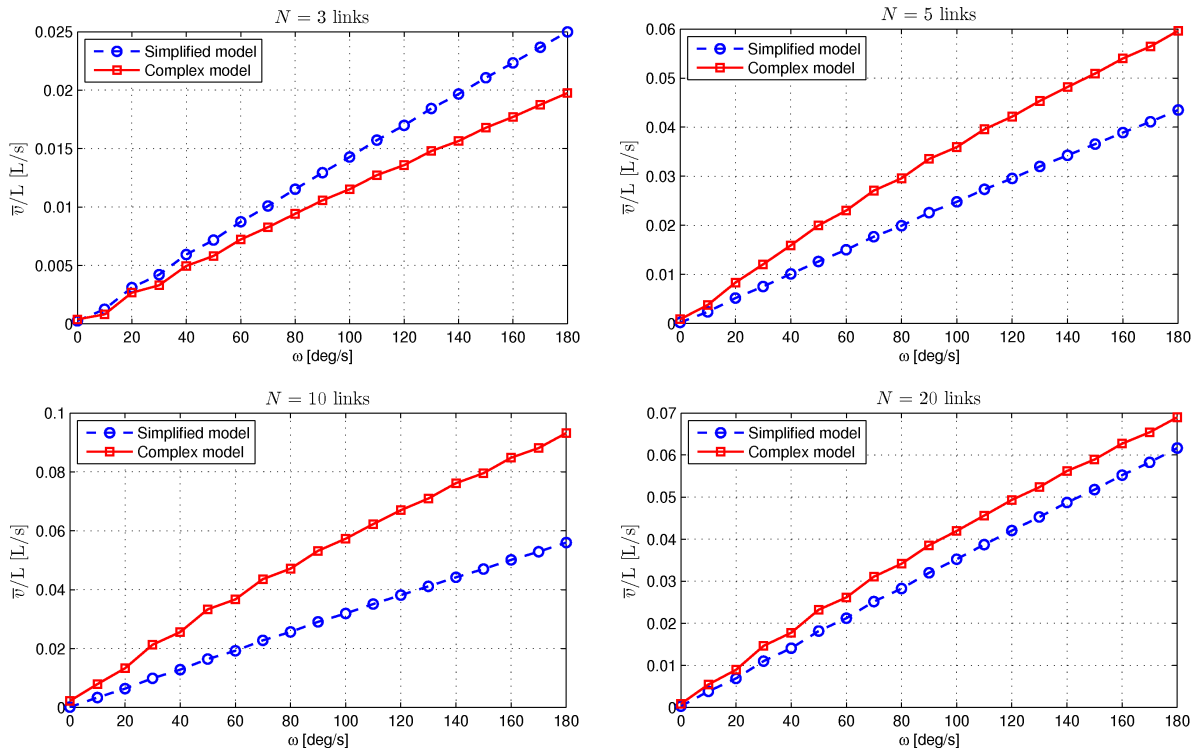
Fig. 23. The forward velocity of the snake robot for different values of ω. The number of links N are shown at the top of each plot.

with different values of ω and calculating the resulting average forward velocity. We considered snake robots with $N = 3$, 5, 10, and 20 links, respectively, where the phase shift was $\delta = 90°$, $50.4°$, $24.1°$, and $11.5°$, respectively. Furthermore, the amplitude of the joint motion was $\alpha = 40°$, $40°$, $30°$, and $10°$, respectively, in the complex model and $\alpha = 5$ cm in the simplified model. The simulation results from the simplified and the complex model are shown in Fig. 23. The linear increase in the forward speed as the frequency ω increases is clearly present in the plots from both models, which is in accordance with Proposition 22.

D. Relationship between the forward velocity and δ

The final result stated in Proposition 22 is that the average forward velocity is maximized by the phase shift δ that maximizes the function k_δ. To investigate the validity of this result, we simulated the snake robot with different values of δ to identify the phase shift that produced the highest forward velocity. We considered snake robots with $N = 3$, 5, 10, and 20 links, respectively, where the amplitude of the joint motion was $\alpha = 40°$, $40°$, $30°$, and $10°$, respectively, in the complex model and $\alpha = 5$ cm in the
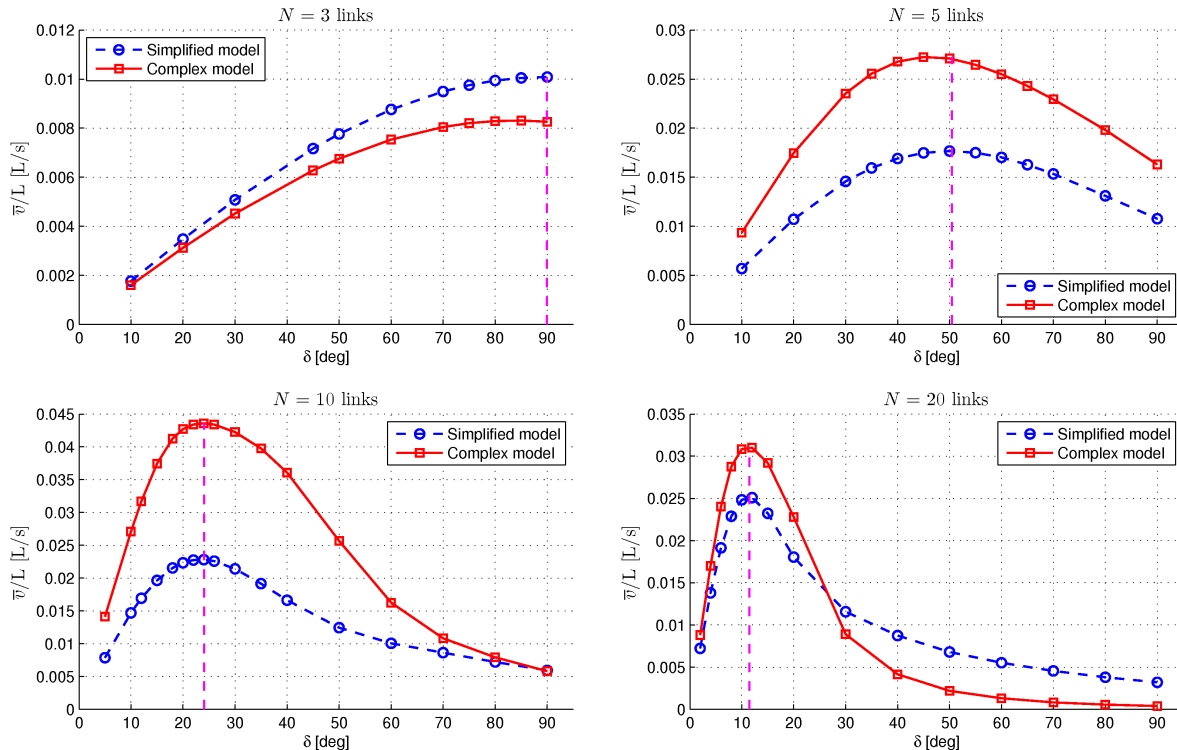
Fig. 24. The forward velocity of the snake robot for different values of δ. The number of links N are shown at the top of each plot. The vertical dashed line indicates the estimated δ value that, by Proposition 22, maximizes the forward velocity.

simplified model. Furthermore, the angular frequency of the joint motion was $\omega = 70°/\text{s}$ in both models. The simulation results from the simplified and the complex model are shown in Fig. 24, where the δ value that maximizes k_δ is indicated with a vertical dashed line in each plot. The maximum velocity of each plot in Fig. 24 seems to agree well with the δ value that maximizes k_δ, which supports the prediction in Proposition 22 concerning the phase shift δ that maximizes the average forward velocity of a snake robot during lateral undulation.

XII. EXPERIMENTAL STUDY: INVESTIGATION OF THE RELATIONSHIPS BETWEEN GAIT PARAMETERS AND FORWARD VELOCITY

This section presents the results from an experimental investigation of the validity of Proposition 22. We first describe the experimental setup and then present the experimental results.

A. The snake robot

The snake robot used in the experiments is shown in Fig. 25(a). A detailed description of the internal components of the robot has been presented in previous literature[38]. The snake robot consists of 10

TABLE III

PARAMETERS OF A JOINT MODULE.

Parameter	Value
Total weight of a joint module	960 g
Outer diameter	130 mm
Degrees of freedom	2
Max joint travel	$\pm 45°$
Max continuous joint torque	4.5 Nm
Max joint speed (no load)	$70°/_{\text{sec}}$

identical joint modules characterized by the parameters listed in Table III. The articulation mechanism of a joint module consists of two links that can move in pitch and yaw, respectively. The links are supported by bearings in a steel ring and have orthogonal and intersecting axes of rotation. The diameter of the steel ring is 130 mm. Each link is driven by a Hitec servo motor (HS-5955TG) and the angle of the links are measured with magnetic rotary encoders (AS5043 from austriamicrosystems).

As shown to the left in Fig. 25(c), each joint module of the robot is enclosed by a plastic ring mounted with 12 plastic wheels. These wheels ensure that the ground friction forces acting on the snake robot are *anisotropic*, i.e. that the friction coefficient characterizing the ground friction forces in the normal (sideways) direction of each joint is larger than the friction coefficient characterizing the ground friction forces in the tangential (forward) direction of the joint. This property is essential for efficient snake locomotion on a planar surface and is also present in the model of the snake robot presented in Section V. Note that the wheels are able to slip sideways, so they do not introduce nonholonomic constraints in the system.

Each joint module is battery-powered and contains a custom-designed microcontroller card used to control the joint angles. A microcontroller card (the brain card) located in the head of the snake robot transmits joint reference angles to all joint modules over a CAN bus running through the robot. The joint reference angles are calculated on an external computer in accordance with a defined control strategy and sent to the brain card via a wireless connection based on Bluetooth. The refresh rate for the two reference angles of each joint module is about 20 Hz. A proportional controller is implemented in the

microcontroller of each joint module in order to control the link angles in accordance with the reference angles.

B. The camera-based position measurement system

During the experiments, the snake robot moved on a white horizontal surface measuring about 240 cm in width and 600 cm in length. This is shown in Fig. 25(b). In order to measure the 2D position of the snake robot during the experiments, we employed the open source camera tracking software *SwisTrack*[39]. Three firewire cameras (Unibrain Fire-i 520c) were mounted in the ceiling above the snake robot as shown in Fig. 25(b). The use of multiple cameras allowed for position measurements over a greater distance than the area covered by a single camera. The cameras were mounted facing downwards approximately 218 cm above the floor and 132 cm apart. The distance between the cameras was chosen so that there was a slight overlap between the images from two neighbouring cameras.

SwisTrack was configured to track black circular markers (40 mm in diameter) mounted on the snake robot as shown to the right in Fig. 25(c). The conversion from the pixel position of a marker to the real-world position (in cm) was conducted by SwisTrack based on a specific calibration method available in this software. SwisTrack estimated the maximum position error to be about 1.9 cm and the average position error to be about 0.6 cm. Each firewire camera was sampled at 15 frames per second. We ran three separate instances of SwisTrack in order to process data from all three cameras and developed our own software in order to merge the output from each SwisTrack instance into the final position measurement of the snake robot. The position of the single marker mounted on the foremost module of the robot was used to represent the measured position of the snake.

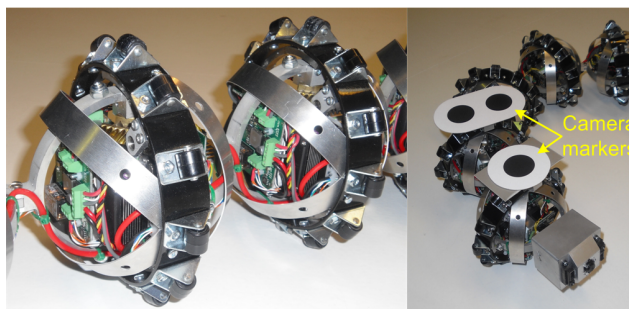## C. Layout of the experiment

The aim of the experiment was to investigate the validity of Proposition 22, i.e. to investigate the relationship between the average forward velocity and the controller parameters of the snake robot during lateral undulation. During the experiment, the joint reference angles were calculated on an external computer and sent to the snake robot through the wireless Bluetooth connection. The reference angles corresponding to the horizontal joint motion of the robot were calculated according to (6) with $N = 10$ links. The reference angles corresponding to the vertical joint motion were set to zero. The resulting position of the robot was recorded by the camera system and the average forward velocity was calculated after each run as the travelled distance divided by the travel time.
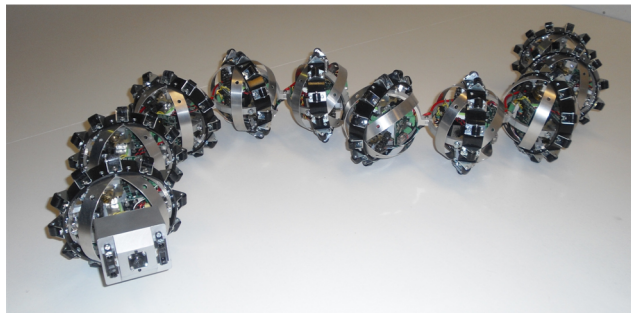
(a) The snake robot used in the experiments.
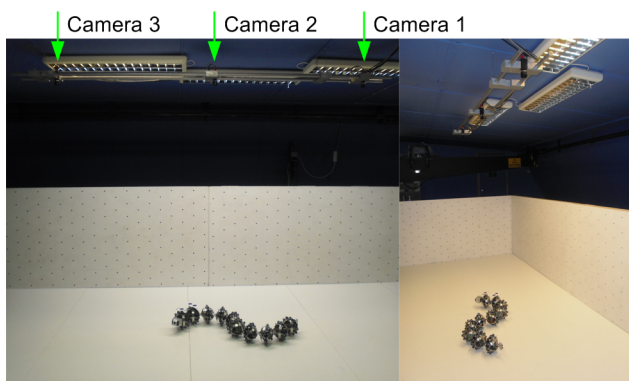
(b) Three cameras mounted in the ceiling measured
the position of the snake robot on the horizontal
surface.

(c) Left: The wheels installed around each joint
module to give the robot anisotropic ground friction
properties. Right: The camera markers mounted to
the robot.
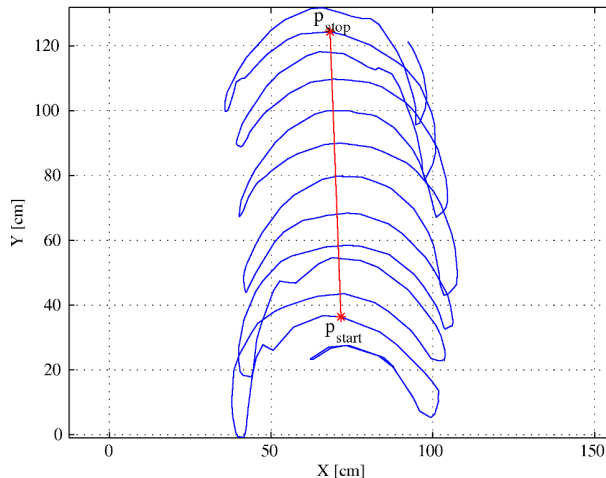
Fig. 25.   The experimental setup.

Fig. 26. A typical plot of the measured position of the snake robot during lateral undulation. The distance between the markers p_{start} and p_{stop} represents the distance travelled by the snake robot.

A typical plot of the measured position of the snake robot from a single run is shown in Fig. 26, which shows that the foremost joint module moves from side to side along the X direction, but has a steady increase in the position along the Y direction. The markers p_{start} and p_{stop} in the plot have been placed near the beginning and near the end of the dataset, respectively, at the approximate center point of the cyclic sideways motion of the snake. We used the distance between these two markers to represent the distance travelled by the snake robot and calculated the travel time as the difference in sample time between the position measurements corresponding to the two markers. The average forward velocity of the snake robot was then calculated as

$$\overline{v} = \frac{\sqrt{(p_{\text{stop},x} - p_{\text{start},x})^2 + (p_{\text{stop},y} - p_{\text{start},y})^2}}{t_{\text{stop}} - t_{\text{start}}} \tag{83}$$

When the duration, $t_{\text{stop}} - t_{\text{start}}$, of a single run of the robot is long, we conjecture that the accuracy of this velocity estimate will be sufficient for investigating the validity of Proposition 22. We developed a special software based on *Matlab* in order to easily identify the markers p_{start} and p_{stop} in the position plot from each run of the robot.

D. Experimental results

The following presents the results from the experimental investigation of the validity of Proposition 22.
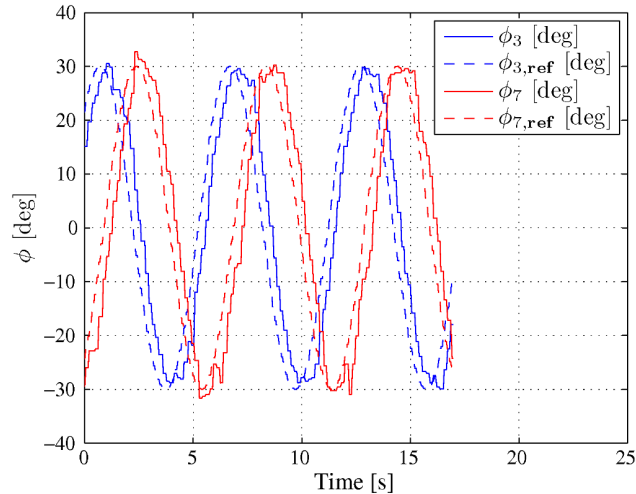
Fig. 27. A plot of the measured (solid) and the corresponding reference angles (dashed) of joint 3 and joint 7 during lateral undulation.

1) Performance of the joint angle controller: In order to show that the joint modules were able to track their joint reference angles, we provide in Fig. 27 a plot of the measured and the corresponding reference angles of two arbitrarily chosen joints (joint 3 and joint 7) during a run of lateral undulation with the snake robot. The plot indicates that the tracking of the joint reference angles is satisfactory.

2) Relationship between the forward velocity and α: Proposition 22 states that the average forward velocity of a planar snake robot is proportional to the squared amplitude of the sinusoidal joint motion, α^2. We investigated the validity of this result by running the snake robot with different values of α and calculating the resulting average forward velocity according to (83). For each value of α, we ran the snake robot three times in order to get multiple velocity measurements. The remaining controller parameters were set to $\omega = 80°$/s, $\delta = 25°$ and $\phi_o = 0°$. Fig. 28 presents the experimental results together with a dashed line between the average of the three velocities measured for each value of α. The plot shows a quadratic increase in the forward speed $\overline{v}$ as the amplitude α increases. This is in accordance with Proposition 22.

3) Relationship between the forward velocity and ω: Proposition 22 states that the average forward velocity of a planar snake robot is proportional to the angular frequency, ω, of the joint motion. This result was investigated by running the snake robot with different values of ω and calculating the resulting average forward velocity according to (83). For each value of ω, we ran the snake robot three times in order to get multiple velocity measurements. The remaining controller parameters were set to $\alpha = 30°$,
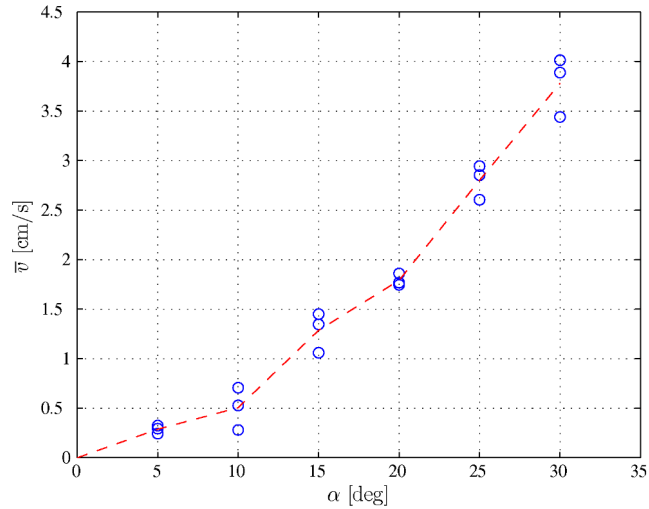
Fig. 28. Experimental result. The average forward velocity of the snake robot from three trials at different values of α and with $\omega = 80°$/s, $\delta = 25°$, and $\phi_o = 0°$.

Fig. 29. Experimental result. The average forward velocity of the snake robot from three trials at different values of ω and with $\alpha = 30°$, $\delta = 25°$, and $\phi_o = 0°$.

$\delta = 25°$ and $\phi_o = 0°$. Fig. 29 presents the experimental results together with a dashed line between the average of the three velocities measured for each value of ω. The plot clearly shows a linear increase in the forward speed $\overline{v}$ as the frequency ω increases. This is in accordance with Proposition 22.
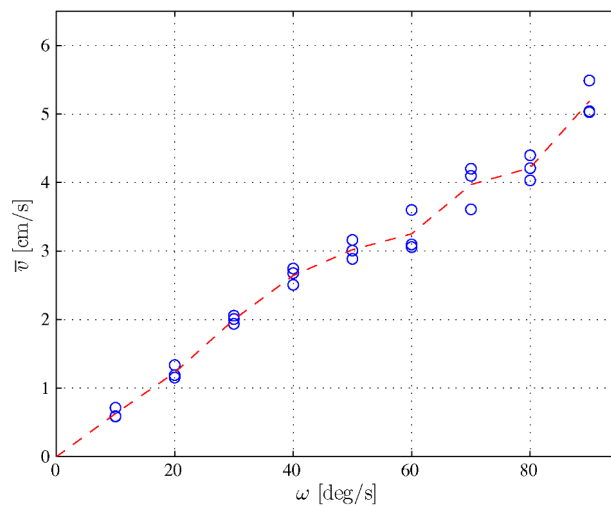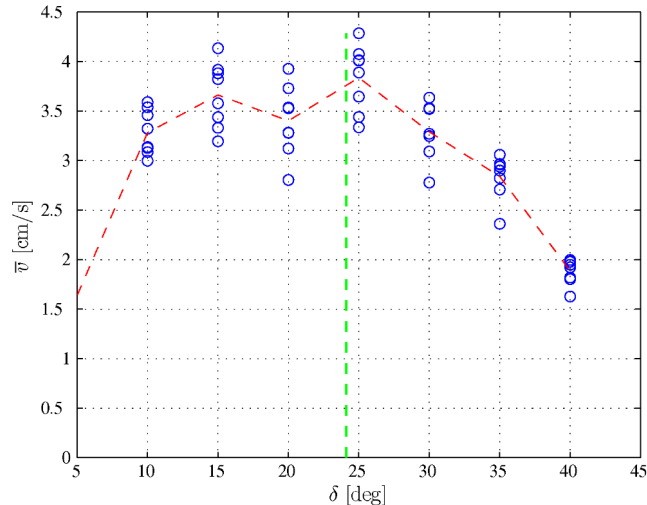
Fig. 30. Experimental result. The average forward velocity of the snake robot from eight trials at different values of δ and with $\alpha = 30°$, $\omega = 80°/s$, and $\phi_o = 0°$.

4) Relationship between the forward velocity and δ: The final result stated in Proposition 22 is that the average forward velocity is maximized by the phase shift δ that maximizes the function k_δ. To investigate the validity of this result, we ran the snake robot with different values of δ to identify the phase shift that produced the highest forward velocity. For each value of δ, we ran the snake robot eight times in order to get multiple velocity measurements. The remaining controller parameters were set to $\alpha = 30°$, $\omega = 80°/s$ and $\phi_o = 0°$. Fig. 30 presents the experimental results together with a dashed line between the average of the eight velocities measured for each value of δ. The δ value that maximizes k_δ for $N = 10$ links is $\delta = 24.1°$, and is indicated with a vertical dashed line in Fig. 30. The plot indicates that the phase shift $\delta = 25°$ produced the highest forward velocity. This agrees well with the phase shift $\delta = 24.1°$ that maximizes k_δ. The average velocity of the eight trials at $\delta = 25°$ was slightly below 4 cm/s. In summary, the experimental results indicate that Proposition 22 provides a reasonable prediction of the phase shift, δ, that maximizes the average forward velocity of a planar snake robot during lateral undulation.

XIII. CONCLUSIONS

This paper has presented several theoretical results aimed at contributing to the understanding of snake robot locomotion. The first contribution of the paper has been a simplified model of lateral undulation dynamics developed for control design and stability analysis purposes. The basic idea behind the model is

to capture only the essential properties of snake robot dynamics, i.e. the features that determine the overall behaviour of the snake. While previous snake robot models describe the body shape dynamics in terms of the *rotational* motion of the links, which generally results in complex equations of motion, the model proposed in this paper describes the body shape dynamics in terms of the *translational* motion of the links, which significantly simplifies the equations of motion. There are several limitations of this modelling approach, which have been elaborated in the paper. In particular, the model is only quantitatively similar to conventional snake robot models as long as the link angles are limited. Moreover, the rotation dynamics of the snake robot is characterized by two general parameters which must be set appropriately in order for the rotational motion to be quantitatively valid. However, since the model was developed to directly capture qualitative properties of snake robot dynamics, we conjecture that the model in general will be *qualitatively* similar to conventional snake robot models.

The second contribution has been an analysis of the simplified model that showed that any asymptotically stabilizing control law for the snake robot to an equilibrium point must be time-varying. Furthermore, the analysis showed that the snake robot (with four links) is strongly accessible from almost any equilibrium point, except for certain singular configurations, and that the robot does not satisfy sufficient conditions for small-time local controllability (STLC). The authors have previously arrived at similar conclusions by analysing a conventional model of a snake robot, which supports the conjecture that the simplified model proposed in this paper captures the essential part of the dynamics of planar snake locomotion.

The third contribution has been an investigation of the velocity dynamics of a snake robot during lateral undulation based on averaging theory that proved that the average velocity of the robot will converge exponentially fast to a steady state velocity. Explicit analytical relations between the steady state velocity and the amplitude, frequency, phase shift and offset of the joint motion during lateral undulation were given. Furthermore, the averaging analysis revealed a set of fundamental relationships between the gait parameters of lateral undulation and the resulting forward velocity of the snake robot. In particular, the derived properties state that the average forward velocity of a snake robot 1) is proportional to the squared amplitude of the sinusoidal motion of each joint, 2) is proportional to the angular frequency of the sinusoidal motion of each joint, 3) is proportional to a particular function of the constant phase shift between the joints, and 4) is maximized by the phase shift between the joints that also maximizes the particular phase shift function.

The paper has presented simulation results and results from experiments with a physical snake robot which supported the theoretical findings.

REFERENCES

[1] J. Gray, "The mechanism of locomotion in snakes," *J. Exp. Biol.*, vol. 23, no. 2, pp. 101–120, 1946.

[2] S. Hirose, *Biologically Inspired Robots: Snake-Like Locomotors and Manipulators*. Oxford: Oxford University Press, 1993.

[3] G. S. Chirikjian, "Theory and applications of hyper-redundant robotic manipulators," Ph.D. dissertation, California Institute of Technology, Pasadena, California, 1992.

[4] G. Chirikjian and J. Burdick, "The kinematics of hyper-redundant robot locomotion," *IEEE Trans. Robot. Autom.*, vol. 11, no. 6, pp. 781–793, December 1995.

[5] J. P. Ostrowski, "The mechanics and control of undulatory robotic locomotion," Ph.D. dissertation, California Institute of Technology, 1996.

[6] P. Prautsch and T. Mita, "Control and analysis of the gait of snake robots," in *Proc. IEEE Int. Conf. Control Applications*, Kohala Coast, HI USA, 1999, pp. 502–507.

[7] S. Ma, "Analysis of creeping locomotion of a snake-like robot," *Adv. Robotics*, vol. 15, no. 2, pp. 205–224, 2001.

[8] H. Date, M. Sampei, and S. Nakaura, "Control of a snake robot in consideration of constraint force," in *Proc. IEEE Int. Conf. on Control Applications*, 2001, pp. 966–971.

[9] M. Saito, M. Fukaya, and T. Iwasaki, "Serpentine locomotion with robotic snakes," *IEEE Contr. Syst. Mag.*, vol. 22, no. 1, pp. 64–81, February 2002.

[10] G. P. Hicks, "Modeling and control of a snake-like serial-link structure," Ph.D. dissertation, North Carolina State University, 2003.

[11] M. Nilsson, "Serpentine locomotion on surfaces with uniform friction," in *Proc. IEEE/RSJ Int. Conf. Intelligent Robots and Systems*, 2004, pp. 1751–1755.

[12] F. Matsuno and H. Sato, "Trajectory tracking control of snake robots based on dynamic model," in *Proc. IEEE Int. Conf. on Robotics and Automation*, 2005, pp. 3029–3034.

[13] A. A. Transeth, N. van de Wouw, A. Pavlov, J. P. Hespanha, and K. Y. Pettersen, "Tracking control for snake robot joints," in *Proc. IEEE/RSJ Int. Conf. Intelligent Robots and Systems*, San Diego, CA, USA, Oct-Nov 2007, pp. 3539–3546.

[14] J. Li and J. Shan, "Passivity control of underactuated snake-like robots," in *Proc. 7th World Congress on Intelligent Control and Automation*, June 2008, pp. 485–490.

[15] D. Hu, J. Nirody, T. Scott, and M. Shelley, "The mechanics of slithering locomotion," in *Proc. National Academy of Sciences, USA*, vol. 106, 2009, p. 1008110085.

[16] R. Hatton and H. Choset, "Approximating displacement with the body velocity integral," in *Proc. Robotics: Science and Systems*, 2009.

[17] P. Liljebäck, K. Y. Pettersen, Ø. Stavdahl, and J. T. Gravdahl, "Controllability and stability analysis of planar snake robot locomotion," *IEEE Trans. Automatic Control*, vol. 56, no. 6, pp. 1365–1380, 2011.

[18] P. A. Vela, K. A. Morgansen, and J. W. Burdick, "Underwater locomotion from oscillatory shape deformations," in *Proc. IEEE Conf. Decision and Control*, vol. 2, Dec. 2002, pp. 2074–2080.

[19] K. McIsaac and J. Ostrowski, "Motion planning for anguilliform locomotion," *IEEE Trans. Rob. Aut.*, vol. 19, no. 4, pp. 637–652, 2003.

[20] K. Morgansen, B. Triplett, and D. Klein, "Geometric methods for modeling and control of free-swimming fin-actuated underwater vehicles," *IEEE Trans. Robotics*, vol. 23, no. 6, pp. 1184–1199, Dec 2007.

[21] P. Liljebäck, K. Y. Pettersen, Ø. Stavdahl, and J. T. Gravdahl, *Snake Robots - Modelling, Mechatronics, and Control*, ser. Advances in Industrial Control.   Springer, 2012.

[22] P. A. Vela, K. A. Morgansen, and J. W. Burdick, "Second order averaging methods for oscillatory control of underactuated mechanical systems," in *Proc. American Control Conference*, vol. 6, 2002, pp. 4672–4677.

[23] J. B. Melli, C. W. Rowley, and D. S. Rufat, "Motion planning for an articulated body in a perfect planar fluid," *SIAM J. Applied Dynamical Systems*, vol. 5, no. 4, pp. 650–669, 2006.

[24] J. Yu, L. Wang, J. Shao, and M. Tan, "Control and coordination of multiple biomimetic robotic fish," *IEEE Trans. Control Systems Technology*, vol. 15, no. 1, pp. 176–183, 2007.

[25] P. Liljebäck, K. Y. Pettersen, Ø. Stavdahl, and J. T. Gravdahl, "A simplified model of planar snake robot locomotion," in *Proc. IEEE/RSJ Int. Conf. Intelligent Robots and Systems*, Taipei, Taiwan, 2010, pp. 2868–2875.

[26] ——, "Stability analysis of snake robot locomotion based on averaging theory," in *Proc. IEEE Conf. Decision and Control*, Atlanta, GA, USA, 2010, pp. 1977–1984.

[27] ——, "Fundamental properties of snake robot locomotion," in *Proc. IEEE/RSJ Int. Conf. Intelligent Robots and Systems*, Taipei, Taiwan, 2010, pp. 2876–2883.

[28] ——, "Experimental investigation of fundamental properties of snake robot locomotion," in *Proc. IEEE Int. Conf. Control, Automation, Robotics, and Vision (ICARCV)*, Singapore, 2010, pp. 187–194, Finalist for the Best Paper Award.

[29] H. K. Khalil, *Nonlinear Systems*, 3rd ed.   Prentice Hall, 2002.

[30] M. Sfakiotakis and D. Tsakiris, "Biomimetic centering for undulatory robots," *The Int. Journal of Robotics Research*, vol. 26, pp. 1267–1282, 2007.

[31] K. Y. Pettersen and O. Egeland, "Exponential stabilization of an underactuated surface vessel," in *Proc. 35th IEEE conf. Decision and Control*, vol. 1, December 1996, pp. 967–972.

[32] R. Brockett, "Asymptotic stability and feedback stabilization," *Differential Geometric Control Theory*, pp. 181–191, 1983.

[33] J.-M. Coron and L. Rosier, "A relation between continuous time-varying and discontinuous feedback stabilization," *J. of Mathematical Systems, Estimation, and Control*, vol. 4, no. 1, pp. 67–84, 1994.

[34] H. Nijmeijer and A. v. d. Schaft, *Nonlinear Dynamical Control Systems*. New York: Springer-Verlag, 1990.

[35] H. J. Sussmann, "A general theorem on local controllability," *SIAM Journal on Control and Optimization*, vol. 25, no. 1, pp. 158–194, 1987.

[36] R. M. Bianchini and G. Stefani, "Graded approximations and controllability along a trajectory," *SIAM J. Control and Optimization*, vol. 28, no. 4, pp. 903–924, 1990.

[37] J. A. Sanders, F. Verhulst, and J. Murdock, *Averaging Methods in Nonlinear Dynamical Systems*, 2nd ed., ser. Applied Mathematical Sciences. Springer, 2007, vol. 59.

[38] P. Liljebäck, K. Y. Pettersen, and Ø. Stavdahl, "A snake robot with a contact force measurement system for obstacle-aided locomotion," in *Proc. IEEE Int. Conf. Robotics and Automation*, Anchorage, AK, USA, 2010, pp. 683–690.

[39] T. Lochmatter, P. Roduit, C. Cianci, N. Correll, J. Jacot, and A. Martinoli, "Swistrack - a flexible open source tracking software for multi-agent systems," in *IEEE/RSJ Int. Conf. Intelligent Robots and Systems*, 2008, pp. 4004–4010.